ISSN 0915-633X

NATIONAL INSTITUTE FOR FUSION SCIENCE

Measurement of Profiles of the Space Potential in JIPP T-IIU Tokamak Plasmas by Slow Poloidal and Fast Toroidal Sweeps of a Heavy Ion Beam

Y. Hamada, A. Nishizawa, Y. Kawasumi, K. Narihara, K. Sato, T. Seki, K. Toi, H. Iguchi, A. Fujisawa, K. Adachi, A. Ejiri, S. Hidekuma, S. Hirokura, K. Ida, J. Koong, K. Kawahata, M. Kojima, R. Kumazawa, H. Kuramoto, R. Liang, H. Sakakita, M. Sasao, K.N. Sato, T. Tsuzuki, J. Xu, I. Yamada, T. Watari and I. Negi

(Received – Jan. 10, 1994)

NIFS-273 Feb. 1994

RESEARCH REPORT
NIFS Series

NAGOYA, JAPAN

Measurement of profiles of the space potential in JIPP T-IIU tokamak plasmas by slow poloidal and fast toroidal sweeps of a heavy ion beam

Y.Hamada,A.Nishizawa,Y.Kawasumi,K.Narihara,K.Sato,T.Seki,K.Toi,
H.Iguchi,A.Fujisawa,K.Adachi,A.Ejiri,S.Hidekuma,S.Hirokura,K.Ida,
J.Koong,K.Kawahata,M.Kojima,R.Kumazawa,H.Kuramoto,R.Liang,H.Sakakita
M.Sasao,K.N.Sato,T.Tsuzuki,J.Xu,I.Yamada,T.Watari

National Institute for Fusion Science
Nagoya, 464-01, Japan

I. Negi

Plasma Physics Laboratory, Kyoto University
Uji, Kyoto, 611, Japan

By the use of simultaneous fast toroidal and slow poloidal sweeps of a heavy ion beam, plasma potential profiles in JIPP T-IIU tokamak are measured at the rate of 120 spatial profiles per second. A new method to eliminate the error due to the change of out-of-plane entrance angle caused by large plasma current, is successfully applied. One of the key factors is the very homogeneous characteristics of the energy analyzer along the wide slit length. A shaped electrode system, instead of guard rings with a resistor chain, successfully increases the homogeneity of an analyzer. The error due to the significant change of an in-plane entrance angle during a poloidal sweep is carefully minimized and calibrated by a secondary beam ionized by neutral gas introduced in a vacuum vessel. The depth of the measured potential at the plasma center reaches more than 1.5 keV in ohmic plasmas with the ion temperature of 600 eV. In some cases, a rather wide region of positive potential and a sharp decrease of the potential in the center of the plasma are observed.

Keywords, HIBP, potential, tokamak, analyzer, beam

§1. Introduction

The heavy ion beam probe(HIBP) in a magnetic confinement system is particularly useful for the measurement of local electric potential and fluctuations of local plasma density and potential.[1] The first precise measurement of a potential profile of a tokamak plasma, was performed in ST tokamak by a single poloidal sweep of a beam across the plasma.[2] Its measurement was, however, conducted at a very low plasma current of about 20 kA where the deviation of the secondary beam from one poloidal plane was very small. It means that trajectories of the beam in the analyzer stay nearly in the analyzer plane (plane of symmetry of the analyzer and perpendicular to the plane of analyzer electrode) because of small deflection due to the plasma current. In this case, the error in the measurement of total energy of the beam is insignificant, since beam velocity perpendicular to the analyzer plane is small. The error is severe in the case of larger plasma current. It is also severe for larger devices because higher beam energy is required. In ISX-B tokamak, potential profiles of ohmic plasmas and beam-heated plasmas with co- and counter-injection, were measured on shot-to-shot basis in order to eliminate the error due to the change in entrance angles.[3] Similar measurements were performed in TM-4 and TEXT tokamaks.[4,5]

In this paper we report the first successful measurement of a potential profile by a single poloidal sweep across the plasma with large plasma current. This is performed by the methods proposed by Y.Hamada *et al.*[6] of the automatic compensation of the error due to out-of-plane entrance angle and careful minimization of the error due to the change of in-plane entrance angle, by the use of the secondary beam ionized by neutral gas puffed into the tokamak vacuum vessel. The automatic compensation of the error due to out-of-plane entrance angle is done by applyig fast toroidal sweeps at the energy analyzer or at the entrance to the tokamak, relying on a simple principle that when the beams enter the energy analyzer at various off-axis entrance angles, a parallel plate analyzer records the maximum and total energy only when the beam direction is parallel to an analyzer axis. In one cycle of a fast toroidal sweep of the beam, there are two moments when an off-axis entrance angle is zero and the beam in the analyzer is parallel to the analyzer

plane. This moment should be easily detected, because at these times the detected beam energy is at local maxima during one toroidal sweep. We could get a potential profile across the plasma in a slow single poloidal and fast toroidal simultaneous sweeps, by connecting these maxima.

An energy analyzer with very homogeneous characteristics along the width of the entrance slit is essential in this method. In our case, the uniform electric field is obtained by the shaped electrode system[7,8] instead of the guard rings with resistor chains since a photocurrent due to the intense plasma radiation flowing to the resistor chain can easily change the uniformity of the electric field. By the combination of these methods, the potential profile measurement with a single poloidal sweep becomes feasible. The details of this method will be discussed in the following section.

§2. Experimental setup and its calibration

The heavy ion beam probe for JIPP T-11U tokamak[9] injects 500 keV thallium ion beam of a few tens of microamperes into the plasma as shown in Fig. 1a.[10] The electrostatic accelerator has a RF driven power supply with very small ripple of less than 2 V_{p-p} at the voltage of 500 kV. Since a cylindrical deflector has very short in-plane focal length and no focal property in out-of-plane movement, two quadrupole lenses are required to focus the beam at the center of the plasma.[7,10] A parallel plate analyzer[11] which has the focus up to the second order, is installed to measure the small change of the secondary beam from the plasma. The amount of its change is equal to the local plasma potential where the ionization occurs as shown in Fig. 1b.

Figures 2a, 2b show the trajectories in x,z vertical plane (a) and in x,y horizontal plane (b), of the primary and secondary beams when the injected 350 keV thallium is swept by a poloidal sweeper.[6] The toroidal magnetic field is 3 Tesla and a plasma current is 200 kA. The symmetry axis of the tokamak is z axis. As the beam is swept by the poloidal sweeper at the entrance to the tokamak, the observation point moves along the observation line and a secondary beam hits the input slit of the energy analyzer at various horizontal positions along the slit and with the various

in-plane and out-of-plane entrance angles. The change of the in-plane entrance angle during a poloidal sweep is about ±3° in the case of Fig. 2a when the observation point moves within the plasma cross-section.

In the case of transient phenomena like the sweep across the plasma cross-section, the change of the beam energy is usually measured by the shift of the beam position on the detector plates.[12] Its shift s from the center of the detector plates shown in Fig. 3a in an ideal parallel plate analyzer is given by 12)

$$s=2.0\frac{\frac{2V_b\cos^2\varphi_{an}}{ZV_a}H_1\sin2\theta_{an}-(X_d-Y_d\cot\theta_{an})}{1+\sqrt{3}\cot\theta_{an}}, \qquad (1)$$

where V_b is the beam energy incident to the analyzer and V_a is a potential of an upper plate of the analyzer. θ_{an} and φ_{an} are in-plane and out-of-plane entrance angles. Other quantities are shown in Fig. 3a. Although s is proportional to the change of the beam energy, it is also affected by the change of entrance angles. In the case of high voltage HIBP its effect is large compared by the shift by the plasma potential, at the focus even up to the second order, and should be examined in detail. The beam position on the detector plates is given by the difference of the upper and lower detector currents normalized by sum of them (ND) by the following equation,[12]

$$ND=\frac{I_U-I_L}{I_U+I_L}=\frac{s}{2.0w}, \qquad (2)$$

where w is the entrance slit height and I_U and I_L are upper and lower detector currents. ND curves of the ideal parallel plate analyzer when the detector is displaced from the second-order focal point by the distance d_{sd} along the line 30 degrees to the electrode surface as shown in Fig. 3a are described by

$$ND=\frac{1}{w}\frac{\frac{2V_b\cos^2\varphi_{an}}{ZV_a}H_1\sin2\theta_{an}-X_f+Y_f\cot\theta_{an}+\frac{d_{sd}}{2}(\cot\theta_{an}-\sqrt{3})}{(1+\sqrt{3}\cot\theta_{an})}, \qquad (3)$$

where, X_f and Y_f are the values for the second-order focal point. Figure 3b shows ND curves with various distances of d_{sd} for an ideal parallel plate analyzer. Positioning of detecor plates at the second-order focal point[11] (d_{sd} =0) is effectivel for the suppression of the error in the measurement of the energy only when the deviation of an in-plane entrance angle from 30° is small. By the comparison of the portions of ND curves (from A to B for d_{sd} =0 and from C to D for d_{sd} = -2 mm) in Fig. 3b , we see clearly that the second-order focal point is not the position of the detector plates for the minimum error when the change of the entrance angle is about ±3° or larger. Careful adjustment of the center of the entrance angle to 30° and the minimization of the error through a small shift of detector position from the second-order focal point are necessary when the change of the in-plane entrance angle is large.

The change of out-of plane entrance angle in the case of Fig.2b is about 6 degrees i.e. maximum φ_{an} is about 0.1 if the analyzer plane is set at x-z plane. Since s is proportional to $V_b \cos^2(\varphi_{an})$ from Eq. 1, the error ΔE in the measurement of the energy due to an out-of-entrance angle is $\Delta E = -V_b (\varphi_{an})^2$. ΔE can be -5 keV if the beam energy is 500 keV and φ_{an} = 0.1. It is extremely large compared with the plasma potentials of about 1 keV in ISX-B[3] and TEXT[4]. Even if we tune an analyzer plane so that average out-of-plane entrance angle during the poloidal sweep to zero, we can only reduce the maximum entrance angle to half and the maximum error to one fourth.

As a systematic way of the compensation of the error due to finite out-of-plane entrance angle, we applied fast toroidal sweeps at the entrance to the tokamak because the space for installing a toroidal sweeper at the analyzer is not available without large modifications of the diagnostic port for HIBP. Since the magnetic configuration of the tokamak is nearly axisymmetric and its trajectories in the poloidal plane are mainly determined by the toroidal field, a toroidal sweep induces only a small shift of the observation point from one magnetic surface as long as the toroidal sweep angle is not large. During a toroidal sweep there is a moment when the direction of the secondary beam in the energy analyzer is parallel to the analyzer plane. At this moment the detected energy

is the largest, as long as the energy analyzer has uniform characteristics along the width of the slit.[6)]

The energy analyzer appropriate to this method should have a very wide slit (1 mm high and 80 mm wide used in the experiment) and the very homogeneous characteristics along this wide input slit. A shaped electrode system as shown in Fig. 3c, may be the best choice[6,7,8)] since the uniformity of the electric field can be enhanced by the corona rings and is free from the disturbing effect of the photocurrent to the resistor chain of the gird rings. The parameters of the energy analyzer are modified from those of Ref. 8 in order to increase the region of uniform electric field. As is shown in Fig. 3e, the uniformity up to $\Delta\phi/\phi_o = 5.0\times10^{-4}$ is obtained numerically after the optimization of the corona plates, in the entire section of the input slit ±4 cm. ϕ is a calculated electric potential in the analyzer and ϕ_o is the electric potential in the ideal energy analyzer. In addition the region of the uniformity of 5.0×10^{-4} is fairly small in the zone covered by the detector.

As shown in Fig. 3d, there are four tuning mechanisms in the analyzer in order to measure a small change of the energy of the beam. One is the precision slide mount of the detector plates to tune the detector plates to the focus. It moves along the line with 30° to the surface of the electrode, the same angle for the second-order focus. This slide mount is useful for the sensitive measurement of the deviation of the entrance angles from 30°, by the comparison of the signals of detectors at two different positions of the detectors on this slide mount. The accurate measurement of the entrance angles is fundamental for the evaluation of the error in high voltage HIBP. In order to tune the in-plane and out-of-plane entrance angles to the designed values of 30° and 0°, the analyzer can be tilted in two directions. In addition, the parallelism of the middle line between upper and lower detector plates with the horizontal opening of the input slit instead of the electrodes, is crucial when we depend on the homogeneity of analyzer characteristics along entire slit length of 8 cm. Accordingly the mechanism to tune the parallelism is equipped in the analyzer.

Figure 3f shows experimentally obtained ND curves when a primary beam of 25 keV Li beam is injected into the tokamak without plasmas and is guided to the energy analyzer by the 2kG toroidal

field. Also ND curves of an ideal parallel plate analyzer, ND versus in-plane entrance angle as a parameter of the deviation of the detector from the focal point are plotted. The focal point of the analyzer is displaced due to the hole effect of the mesh on the lower electrode as large as 1.5 cm as is shown in Fig. 3f.[16,8] Since the vacuum port is not optimized for the primary beam detection, the range of the entrance angle is limited to rather small value because of the blockage of the beam by the port. We can however, clearly observe that ND curves are very similar to the theoretical curves except the displacement of the focus point.

In order to tune these parameters to minimize the shift of ND curves in a poloidal scan of the observation point, the ionization of thallium beam by neutral gas in the vacuum vessel is employed[6,13] instead of the generation of the secondary beam by a tokamak plasma. The change of the beam energy during the ionization by neutral gas may be the order of the ionization energy of the neutral particle if the neutral gas density is small. It is much smaller than the expected plasma potentials of a few hundred volts. Accordingly, tuning of the analyzer and calibration of the error in the measurement by gas ionization is presently the best *in situ* method. Its signal is, however, small[6] compared with the conventional small gas box, because of the large difference of the length of interaction with neutral gas. Because the cross-section of the recombination of the primary beam is larger than that of the ionization[15] around 400 keV, neutral gas density (proportional to the signal when it is small) is much more severely limited by the multiple process of recombination and ionization of the primary beam[6]. Accordingly, the very accurate calibration is not feasible by gas puffing into the vacuum vessel. It is, however, very important to find out whether or not we tune the detector position and average in-plane entrance angle near the optimal value. In addition, it is very efficient because by one sweep we can determine the error curve. Further we can perform the calibration at each plasma shot after the discharge is terminated, as is performed in ATF.[13]

Figure 4a shows typical time behaviours of the sum of the detector currents and the normalized difference (ND) under 60Hz poloidal sweep after hydrogen gas is introduced into the vacuum vessel by gas puffing. The 400 keV thallium beam is swept at the

entrance to the tokamak in the poloidal direction as shown in Fig. 2a. The toroidal field is 3 Tesla. In Fig. 4a, we can observe that the sum of the detector currents is at first very large (point A) and then decays slowly. It finally decays suddenly (point B). Since the gas density may be considered to be rather homogeneous in the slow transient phenomena, we expect that the signal is proportional to the volume of the observation point (sample volume[7]). The sharp and large peak of the current can be considered to be the divergence of the sample volume. The sharp decay of the signals (point B) in Fig. 4a is considered to be due to the blockage of the beam with the lower part of the horizontal port of the vacuum vessel. It is useful to have these charecteristic points since these points can be used as reference points of the sweep angle and the observation point in the plasma, although at the observation point near the divergence of sample volume, the spatial resolution is very poor. The point of the divergence is inside the vacuum vessel and outside the tokamak plasma. In the case of lower beam energy this phenomenon is not observed due to the collision of a primary beam with the wall of vacuum vessel.

The detailed view of the change of the observation point and the trajectories of the primary and secondary beams during this poloidal scan of Fig. 4a are shown in Fig. 4b. We can see that there are two ionization points which correspond to the input slit of the analyzer on a primary beam trajectory, although most of the trajectories from the upper ionization point are blocked by the wall of the ports as is shown in Fig. 4b or blocked at the opening of the lower electrode of the energy analyzer. There is a poloidal sweep angle where the two birth places merge to one point. This sweep angle may correspond to the divergence of the sample volume. By Fig. 4c we can discuss this phenomenon further.

Figure 4c shows the result of the trajectory calculations; how the secondary beam moves on the slit plane as the place of ionization moves on the trajectory of the primary beam. The abscissa is the radial coordinate of the point where the secondary beam and the slit plane cross. The ordinate is the z coordinate of the birth place of the secondary beam on the primary beam trajectories for various poloidal sweep angles. The slit plane is assumed to be the plane intersecting the input slit and is shown in Fig. 2a. If at certain sweep angle, the radial coordinate of the

opening of the slit point coincides with the point on the curve where the derivative diverges, then the ratio of the slit height to the length of the birth place on the trajectory of the primary beam diverges : the divergence of the sample volume. The poloidal sweep angle of the experimentally observed peak is found to be in agreement with the numerical calculations.

The change of ND of Fig. 4a is a little large because in this case the detector is nearly on the second-order focal point and the entrance angle at the divergence of the sample volume is near 30°. It is roughly explainable from ND curve of the ideal analyzer on the second-order focal point in Fig. 3b (curves from A′ to B′ for d_{sd} =0). Since the behaviours of the ND do not change appreciably during gas puff, we can conclude that ND in Fig.4a is not affected much with multiple ionization and recombination processes.

Figure 5 shows nearly optimal ND curve by the gas ionization after the experimental survey of the detector point and entrance angle. In this case the detector is shifted by about 5 mm along the precision slide mount towards the lower electrode from the focus point and the analyzer is rotated by the angle of 1.5° from the angle of Fig. 4a in order to reduce the entrance angle. The normalized difference is rather noisy because of the small detector currents and rather small smoothing time of 100 μs in this case. In spite of these facts we can see that the change of ND showed smaller value compared with ND curve in Fig. 4a. This result can be roughly explained by Fig. 3b (curves from C′ to D′ for d_{sd} = −4 mm). In addition, the total detector current at the divergence of the sample volume is small compared with the case of Fig. 4a. It is found from the trajectory analysis in the energy analyzer that because of the rotation of the analyzer by 1.5°, the contribution from the upper birth place is completely blocked in the analyzer resulting in the smaller total current in Fig. 5. ND curve almost up to the angle of divergence is therefore, free from the effect of upper birth place and can be used as the calibration curves. The error is reduced to ±200 eV compared to the measured potential of about 1.5 kV at the plasma core as is discussed later. Most of the measurement is done in this configuration and the error due to the change in the in-plane entrance angle is neglected in the analysis.

Figure 6a, b show time behaviours of ND of the gas-ionization currents and a monitor signal of the toroidal sweep voltage under

toroidal sweep when the analyzer axis is shifted by 3.0° for (a) and by -3.0° for (b) in the case of Fig. 4c. The maxima of ND for both cases are approximately the same in spite of the large difference in the toroidal deflection angle under the approximately opposite sweep voltage. It experimentally supports our method of the measurement indicating we can get true total energy even if the beam is under the large toroidal deflections and our energy analyzer has very homogeneous characteristics along the horizontal displacement of the beam at the input slit.

§3. Potential profiles in JIPP T-IIU Plasmas

Figures 7a and 7b show the successive displays of ND of the currents of the upper and lower detector plates, proportional to local plasma potential, as a function of time under poloidal and toroidal sweeps. The observation point in the case of Fig. 7a (400 keV, 3 Tesla) is swept from the plasma boundary to the core region as shown in Fig. 4b, while the observation point in Fig. 7b (250 keV, 3 Tesla) moves from plasma boundary to plasma boundary as shown in Fig. 7c. The poloidal sweep frequency is 60 Hz. 5 kHz fast toroidal sweep is applied for the compensation of the error due to the off-axis entrance angle. As shown in Fig. 7a and Fig. 7b, the local maxima occur at the frequency about 2 times larger than that of the toroidal sweep, since during a toroidal sweep there occurs twice the case when the direction of the beam is parallel to the analyzer plane. These small local peaks (local maxima) of ND during toroidal sweep are the ones predicted in Ref. 6. Since only when the direction of the beam is parallel to the analyzer axis ND (measured energy) is at the local maximum and free from the error due to the out-of-plane entrance angle, the plasma potential is approximately the dashed curve connecting small peaks induced by the toroidal sweep.

The discharge is purely ohmic in this case. Time behaviours of plasma parameters such as plasma current and average density, are shown in Fig. 7d. The center ion temperature determined by the Doppler broadening of FeXX 2665.1 Å is 600±30 eV at the current plateau. We can observe that from Fig. 7a, 7b and 7c that in the early phase of the discharges where plasma current is small, the depth of the plasma potential profiles in the center of the plasma

column is small (first or second ND displays in Fig. 7a and 7b). As plasma current grows, the depth grows steadily. Both reach at steady level 100 ms after the initiation of the discharge. Since the shift of ND at the calibration (Fig. 5) is much smaller than the shift in Fig. 7a at the steady level, we can state that the plasma potential has a fairly large negative potential of more than -1 keV in the center region similar to the previous measurements in ISX-B, TM-4 and TEXT.[3,4,5] In case of Fig. 7b, the plasma potential goes down as the observation point moves from plasma boundary to an interior region and goes up again to almost the initial value as it moves back to plasma boundary. Similarly as the observation point moves toward lower half of the plasma cross-section, the distance from the plasma axis and the plasma potential increase as is shown in the second and third curves of ND of Fig. 7a. The sum of the detector currents, shown in Fig. 7a and 7b shows large attenuation of the beam even in the case of 400 keV thallium beam. It is strongly modulated by large toroidal sweeps because the beam moves on the detector by larger distance than the width of detector plates. The detail of its movement is closely related to the possibility of current profile measurement and will be reported in a separate paper.

The level of plasma potential at plasma boundary varies with time since the high voltage source for the analyzer is a little affected by the intense radiation at the early phase of the discharge. Because the poloidal sweep time across the plasma is much shorter than the characteristic time of the highly stabilized source, the relative change of the plasma potentials from the boundary layer to the plasma center is fairly accurate. Figure 8 shows the radial profiles of the plasma potential calculated by the dependence of the observation point on the sweep angle shown in Fig. 4c.

We happened to observe rather different profiles of the potentials as shown in Fig. 9. The main features of the profiles are wide area of rather positive or flat potential in the outer layer of the plasma column and the sharp decrease of the plasma potentials in the center of the plasma as was observed in TM-4 and TEXT.[4,5] The positive and rather flat region is not affected by the Mirnov oscillations although we can not rule out the possibility of locked mode. This may mean that the turbulence

outside the hot core of the plasma is not due to large-scaled instabilities and has characteristics of larger electron mobility compared to the ion mobility across the magnetic surface. Fig. 9b shows the radial profiles of electron and ion temperature by 28-spatial-points-100Hz YAG Thomson scattering apparatus and the measurement of the Doppler width of various line emissions. The narrow region of hot cores of the plasma column is due to the high q (about 6) operation of the discharge. The radial profiles of the electron temperature are consistent with the prediction of profile consistency. As was stated in TEXT potential measurement[5], we can not switch the discharge deliberately to the one with large positive area from that without it.

In conclusion it is established experimentally that the combination of fast toroidal and slow poloidal sweeps in high voltage HIBP effectively reduces the error due to the change of the out-of-plane entrance angle induced by the plasma current. By this new method the measurement of potential profiles in a single discharge with the rate of 120 profiles per second or more becomes feasible in a large current tokamak discharge.

We would like to thank Director-general A.Iiyoshi and Professors M. Fujiwara and K.Matsuoka for their continuous supports.

References

1) J.C.Jobes,and R.L.Hickok: Nuclear Fusion **10**(1970) 195.

2) J.C.Hosea,F,C.Jobes,R.L.Hickok,and A.N.Dellis: Phys. Rev. Letts. **30** (1973) 839.

3) G.A.Hallock,J.Mathew,W.C.Jennings,R.L.Hickok, K.A.Conner,A.J.Wooton,and R.C.Isler: Phys. Rev. Lett. **56** (1986) 1248.

4) V.I.Bugarya,A.V.Gorshkov,S.A.Grashin,I.V.Ivanov, V.A.Krupin,A.V.Mel'nikov,K.A.Razumova,Yu.A.Sokolov, V.M.Trukhin,A.V.Chankin,P.N.Yushmanov,L.I.Krupnik, I.S.Nedzel'skij: Nuclear Fusion **12** (1985) 1707.

5) X.Z.Yang,B.Z.Zhang,A.J.Wooton,P.M.Schoch,B.Richards,D.Baldwin, D.L.Brower,G.G.Castle,R.D.Hazeltine,J.W.Heard,R.L.Hickok, W.L.Li,H.Lin,S.C.McCool,V.J.Simcic,Ch.P.Ritz, and C.X.Yu: Phys. Fluids **B3** (1991) 3448.

6) Y.Hamada,K.Masai,Y.Kawasumi,H.Iguchi,A.Fujisawa,and JIPP T-11U

Group, J. Plasma and Fusion Research, **69** (1993) 1050.
7) P.M.Schoch,A.Camevali,V.T.P.Crowley,J.C.Forster, R.L.Hickok,J.F.Lewis,and J.G.Schatz,Jr.: Rev. Sci. Instrum. **59** (1988) 1646.
8) Y.Hamada,Y.Kawasumi,K.Masai,H.Iguchi,A.Fujisawa,and JIPPT-llU group, Rev.Sci.Instrum., **63** (1992) 4446.
9) K.Toi,Y.Hamada,K.Kawahata,T.Watari,A.Ando,K.Ida,S.Morita, R.Kumazawa,Y.Oka,K.Masai,M.Sakamoto,K.Adachi,R.Akiyama, S.Hidekuma,S.Hirokura,O.Kaneko,T.Kawamoto,Y.Kawasumi, M.Kojima,T.Kuroda,K.Narihara,Y.Ogawa,K.Ohkubo,S.Okajima, T.Ozaki,M.Sasao,K.Sato,K,N.Sato,T.Seki,F.Shimpo, H,Tanahashi,Y.Taniguchi,T.Tuzuki: *Proc. 13th Int. Conf. on Plasma Physics and Conrolled Nuclear Fusion Research, Washington,D.C., 1990,* Vol. p.301, IAEA, Vienna (1991).
10) Y.Hamada,Y.Kawasumi,M.Masai,H.Iguchi,A.Fujisawa and JIPP T-llU Group: Annual Review of NIFS (1990) p.118.
11) T.S.Green and G.A.Proca: Rev.Sci.Instrum.**41** (1970) 1409.
12) L.Solensten and K.A.Connor: Rev.Sci.Instrum.**58** (1987) 516.
13) S.C.Aceto,K.A.Connor,J.G.Schwelberger,J.Zielinskii, Rev. Sci.Instrum. **63** (1992) 4568.
14) J.Zielinskii,S.C.Aceto,J.G.Schwelberger,K.A.Connor, J.F.Lewis,J.C.Glowienka,A.Carnevali: Rev. Sci. Instrum. **63** (1992) 4574.
15) I.Alvarez and C.Cisneros, Phys. Rev. **13** (1976) 1728.
16) Y.Hamada,Y.Kawasumi,H.Iguchi,A.Fujisawa,Y.Abe and M.Takahashi, Research Report of National Institute for Fusion Science, NIFS-203, December 1992, to be published in Rev. Sci. Instrum.

Figure Captions

Figure 1. a) The experimental setup of a heavy ion beam probe in JIPP T-llU tokamak. b) Schematics of the change of the beam energy on the trajectories of primary and secondary beams. X marks show the point of the ionization of the primary beam by a tokamak plasma or neutral gas.

Figure 2. Trajectories of the primary and secondary thallium ion beam in JIPP T-IIU tokamak under poloidal sweeps at the entrance to

the tokamak. Beam energy is 350 keV and plasma current is 200 kA. 3 Tesla of toroidal field. a) Cross-sectional view, b) Plan view.

Figure 3. Schematics of the parallel plate energy analyzer and its characteristics. a) Schematics of the trajectory of the beam in a parallel plate analyzer. b) Normalized difference ND (difference of the upper and lower detector plate currents normalized by sum of them) of an ideal parallel plate analyzer versus in-plane entrance angle under various distances d_{sd} of the detector from the second-order focal point as is shown in Fig. 3a. The slit height is 1 mm. X_f = 64.95 cm and Y_f = 12.5 cm. d_{sd} is changed by every 2mm. c) Cross-sectional view of the energy analyzer. d) Side view. e) The contour plot of the optimized uniformity of the potential ($10^4\Delta\phi/\phi_o$) near the plane of the analyzer. $\Delta\phi = \phi-\phi_o$, while ϕ is the calculated local potential and ϕ_o is the ideal potential. The uniformity is very high near the electrodes and deteriorates as the distance from the electrodes is large. The optimized length of corona bar is DY=2.78cm, for Av=25 cm, H1=8.5 cm, H2=7.5 cm, S1=18.5 cm, dt=1.5 cm and DX=1.5 cm. f) Normalized difference ND curves of the ideal parallel plate analyzer (simple curves) and the experimentally obtained curves (weaving curves). 25 keV Li primary beam is injected into JIPP T-IIU tokamak with 2kG toroidal field and guided into the analyzer. The slit height is 1 mm. The experimental curves are normalized at q =30°.

Figure 4. a) Typical time behavours of the total detector current generated by neutral gas ionization and ND (normalized difference) under poloidal sweep. Hydrogen gas puff is performed into the tokamak vacuum vessel. The magnetic field strength is 3 Tesla and thallium beam energy is 400 keV. Detector plates are about on a displaced focal point (d_{sd} = 15 mm). b) The detailed view of the change of the observation point and trajectories in case of Fig. 4a near the plasma column. The trajectories of the primary beam swept at the entrance of the tokamak (every 0.5°) and the secondary beams which hit the input slit are shown. c) The distance of the hitting place of the secondary beam on the input-slit plane as a function of the z coordinate of the birth place of the secondary beam under various poloidal sweep angles at the tokamak in the case of Fig. 4a.

Figure 5. Time behaviour of ND of currents due to the gas ionization under poloidal sweep. The detector plates are displaced by about 5 mm from the focal point of Fig. 3f on the slide line 30° to the lower electrode (about d_{sd} = 10 mm). The analyzer is rotated by the angle of 1.5° from the case of Fig. 4a to reduce the entrance angle. Most measurements are performed by this configuration. This ND curve is the calibration curve for the potential measurement. Also the time traces of the total detector current and the poloidal sweep monitor are shown.

Figure 6. Time behaviours of ND of the detector currents by gas ionization under 60 Hz sinusoidal toroidal sweep. The analyzer plane (plane of symmetry of the analyzer) is rotated from the x-z plane by the angle of -3.0° in the case of (a) and 3.0° in the case of (b). The rotation axis is the vertical line at the middle of the entrance slit as shown in Fig. 3d. Also shown is the toroidal sweep voltage monitor.

Figure 7a) and b). Normalized difference (ND) of the detector currents versus time under fast toroidal sweeps at successive poloidal sweeps. Beam energy is 400keV for Fig.7a and 250 keV for 7b. Also total sum of the detector currents (dashed and dotted curve) and a monitor signal of poloidal sweep are included. Plasma potentials are dashed lines connecting the small peaks due to fast toroidal sweeps. Discharge parameters are B_t=3 T, I_{pmax} = 230 kA, a_p=21 cm, R_p=91 cm. c) The detailed view of observation points and trajectories for 250keV beam energy near the plasma column. The primary beam is swept by every 0.5° at the entrance of the tokamak and the secondary beams which hit the input slit are shown. d) Time behaviours of plasma quantities; plasma current, loop voltage, diamagnetism and average plasma density of Fig. 7a.

Figure 8 Successive displays of electric space potential (ND) in a tokamak plasma versus minor radius converted from Fig. 7a. Minor radius is computed from a poloidal sweep monitor using the data of Fig. 4b.

Figure 9 (a) ND of the detector currents versus time under fast toroidal sweeps at successive poloidal sweeps. Small positive potential is observed from the boundary to about r/a_p=0.5. (b) Electron temperature profile and ion temperature at the same condition.

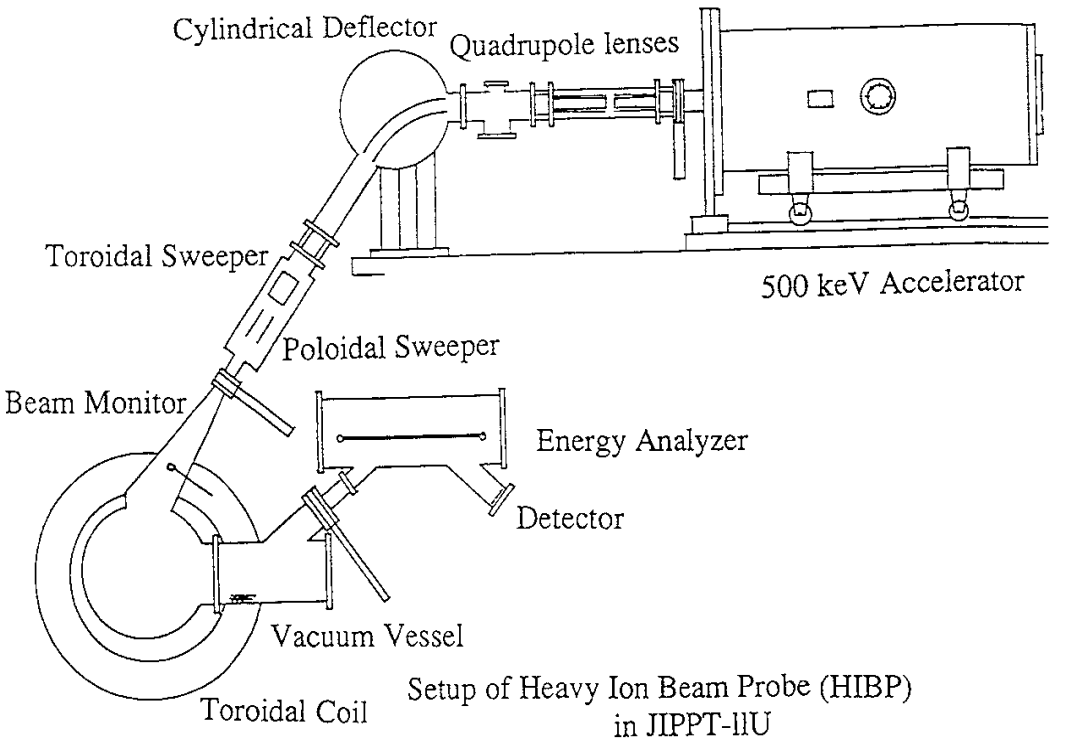
Cylindrical Deflector
Quadrupole lenses
Toroidal Sweeper
500 keV Accelerator
Poloidal Sweeper
Beam Monitor
Energy Analyzer
Detector
Vacuum Vessel
Toroidal Coil
Setup of Heavy Ion Beam Probe (HIBP)
in JIPPT-IIU

(a)

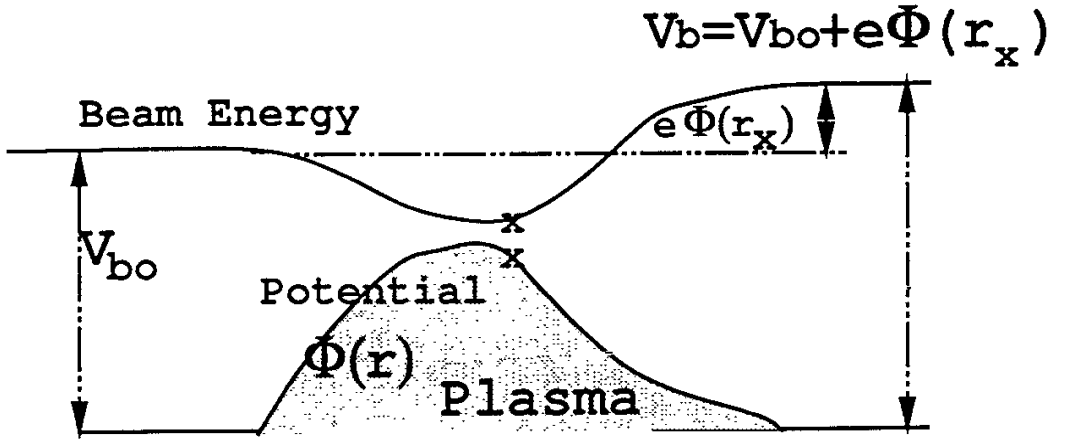
Vb=Vbo+eΦ(rx)
Beam Energy
eΦ(rx)
Vbo
Potential
Φ(r)
Plasma

(b)

Figure 1

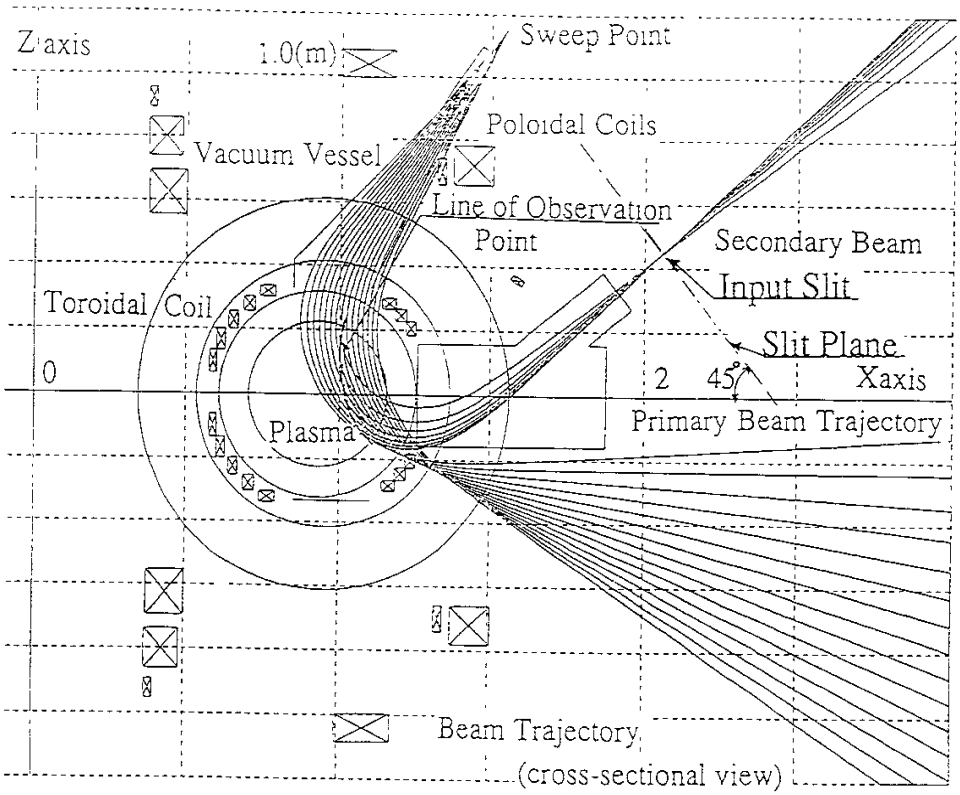
Z axis
1.0(m)
Sweep Point
Poloidal Coils
Vacuum Vessel
Line of Observation
Point
Secondary Beam
Input Slit
Toroidal Coil
Slit Plane
0
2
45°
Xaxis
Primary Beam Trajectory
Plasma
Beam Trajectory
(cross-sectional view)

(a)

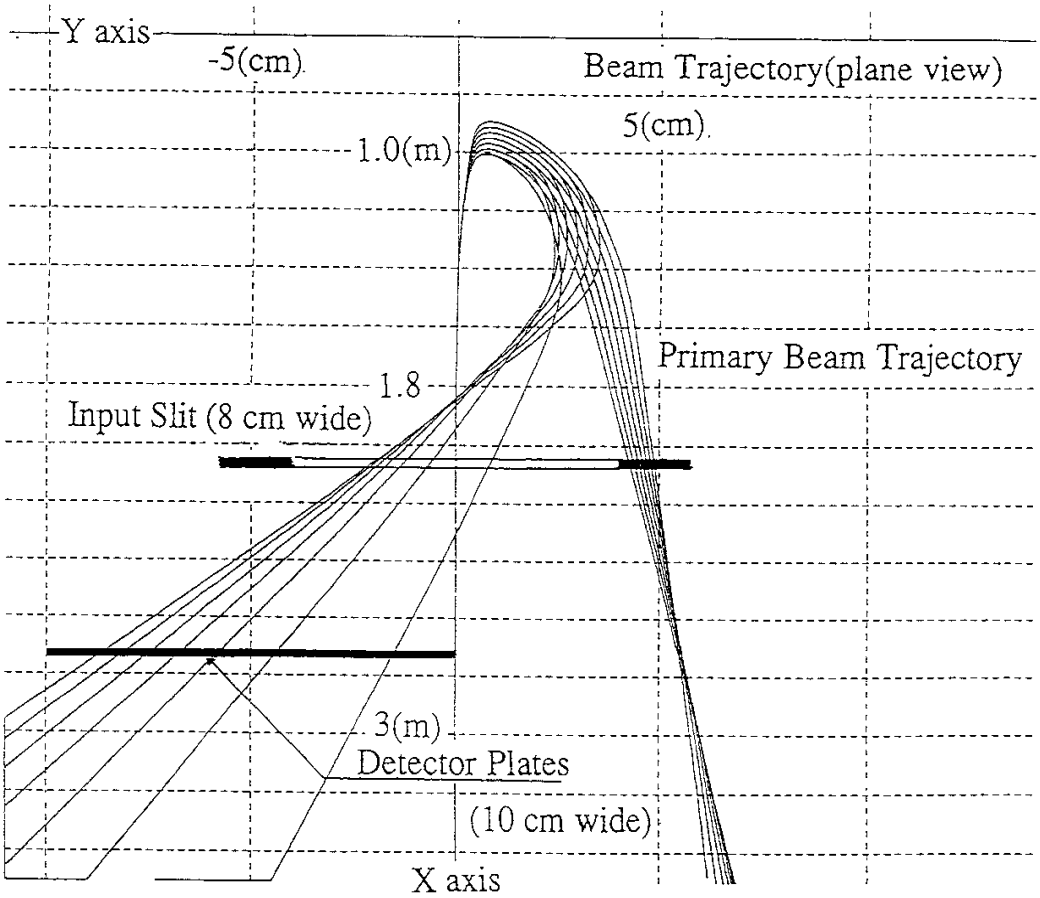
Y axis
-5(cm)
Beam Trajectory(plane view)
5(cm)
1.0(m)
Primary Beam Trajectory
1.8
Input Slit (8 cm wide)
3(m)
Detector Plates
(10 cm wide)
X axis

(b)

Figure 2

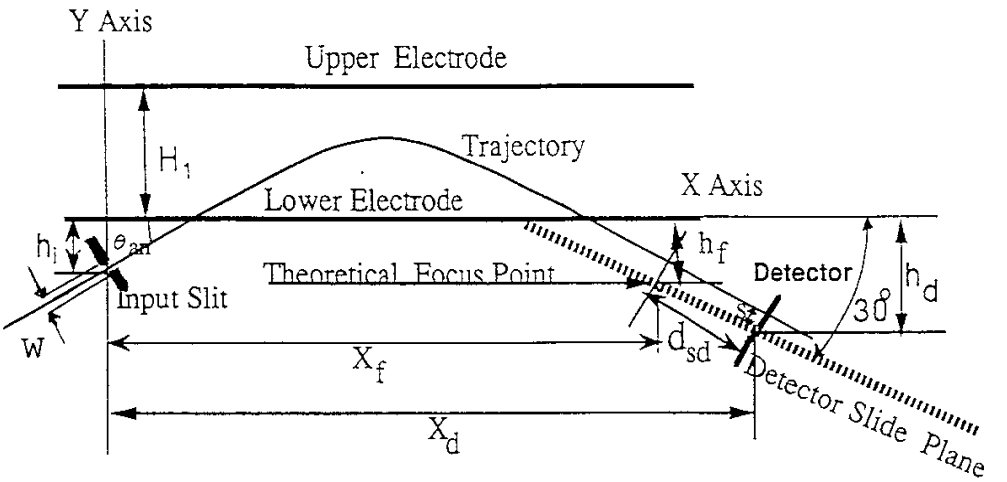

$$Y_d = h_d + h_i$$

$$Y_f = h_f + h_i$$

(a)

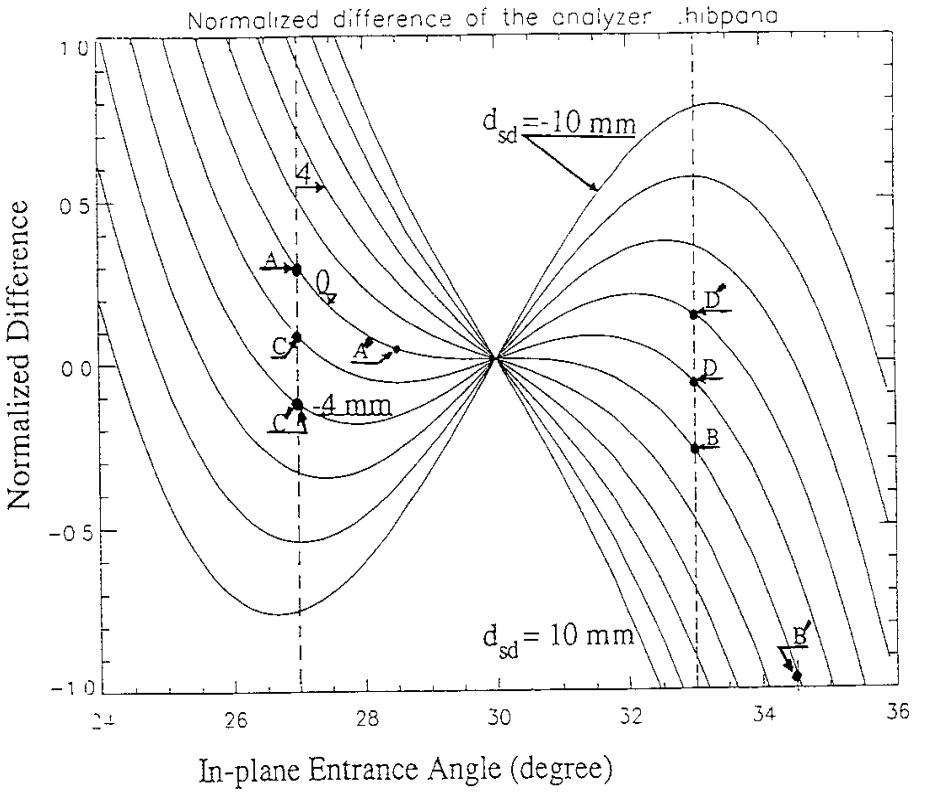

(b)

Figure 3

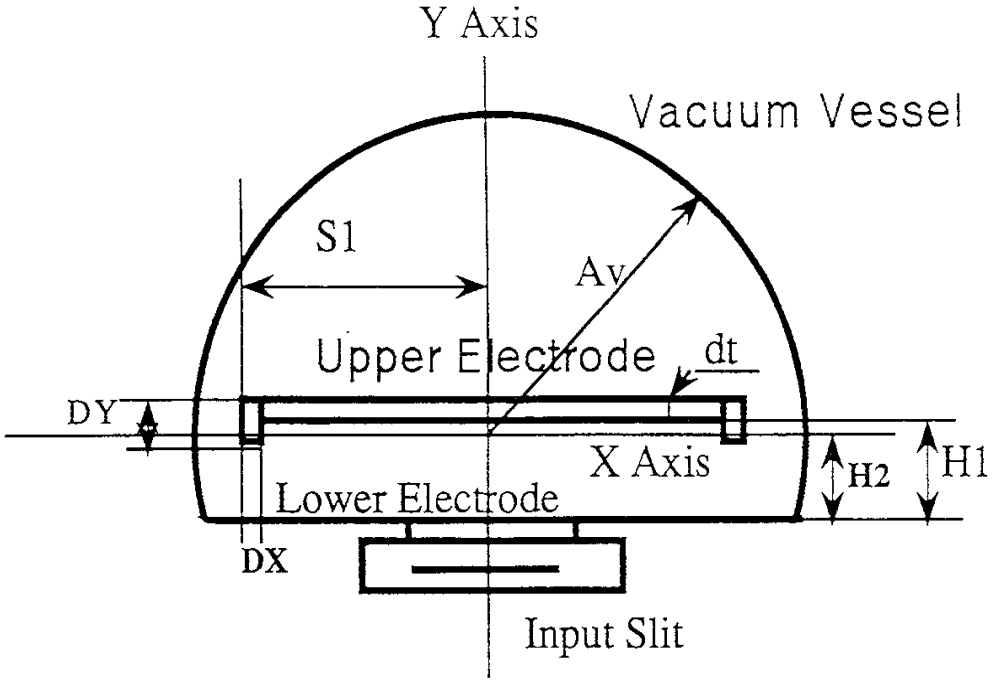
Y Axis
Vacuum Vessel
S1
Av
Upper Electrode
dt
DY
X Axis
H2
H1
Lower Electrode
DX
Input Slit

(c)

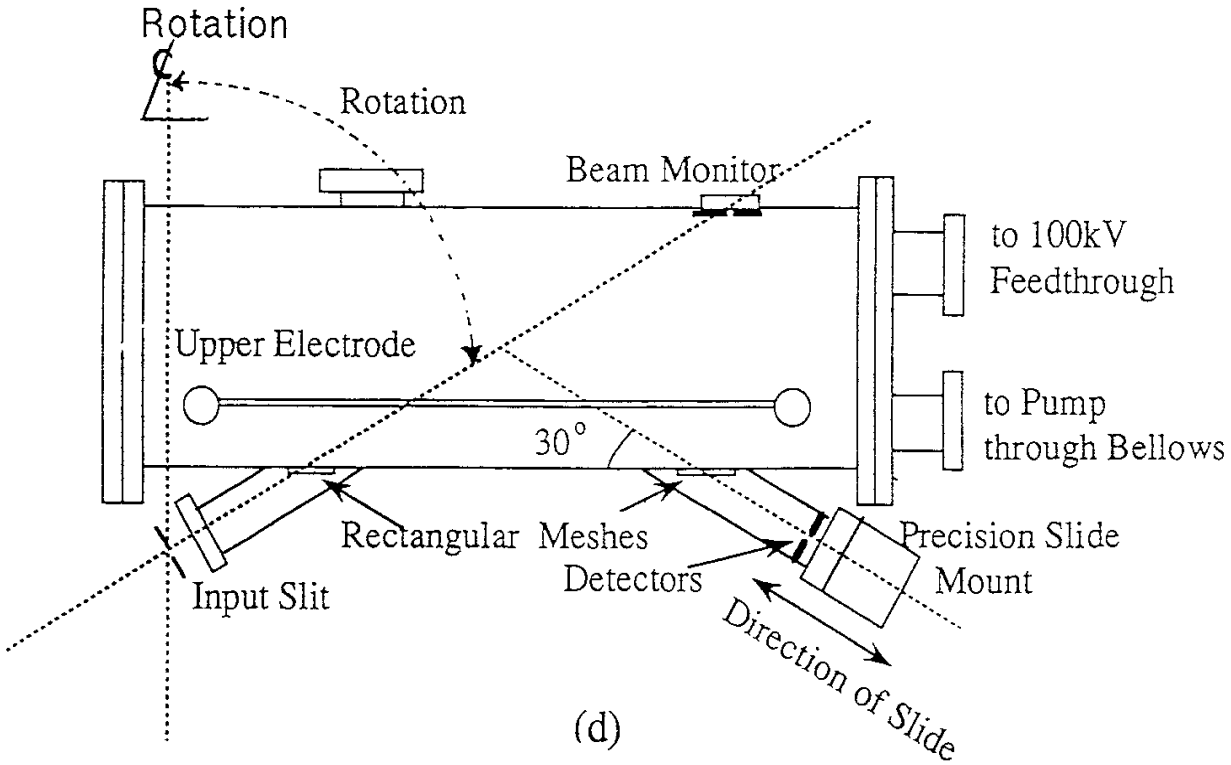
Rotation
Rotation
Beam Monitor
to 100kV
Feedthrough
Upper Electrode
to Pump
through Bellows
30°
Rectangular Meshes
Detectors
Precision Slide
Mount
Input Slit
Direction of Slide

(d)

Figure 3

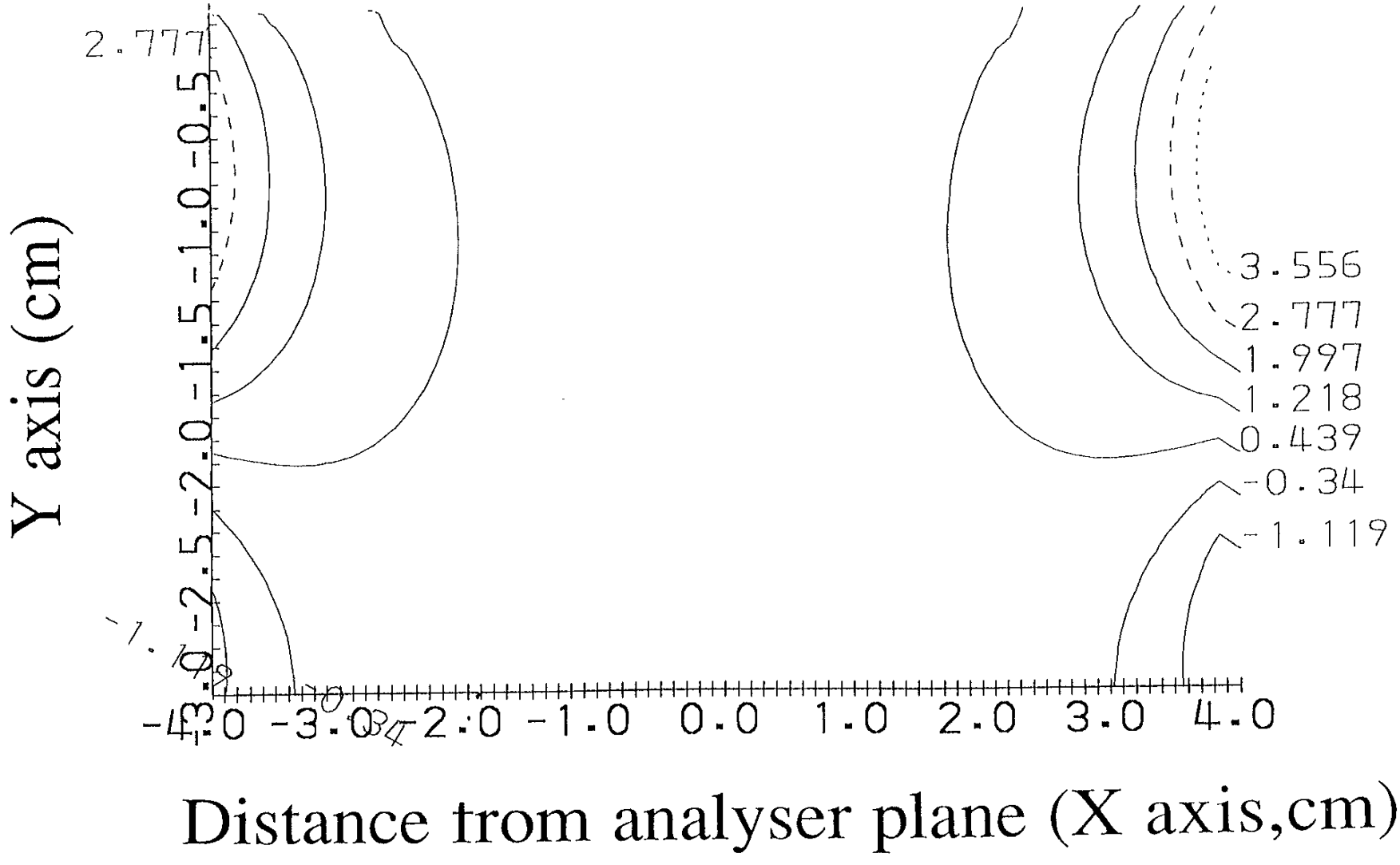
Y axis (cm)
2.777
-0.5
-1.0
-1.5
-2.0
-2.5
-3.0
3.556
2.777
1.997
1.218
0.439
-0.34
-1.119
-4.0
-3.0
-2.0
-1.0
0.0
1.0
2.0
3.0
4.0
Distance from analyser plane (X axis,cm)

Figure 3e

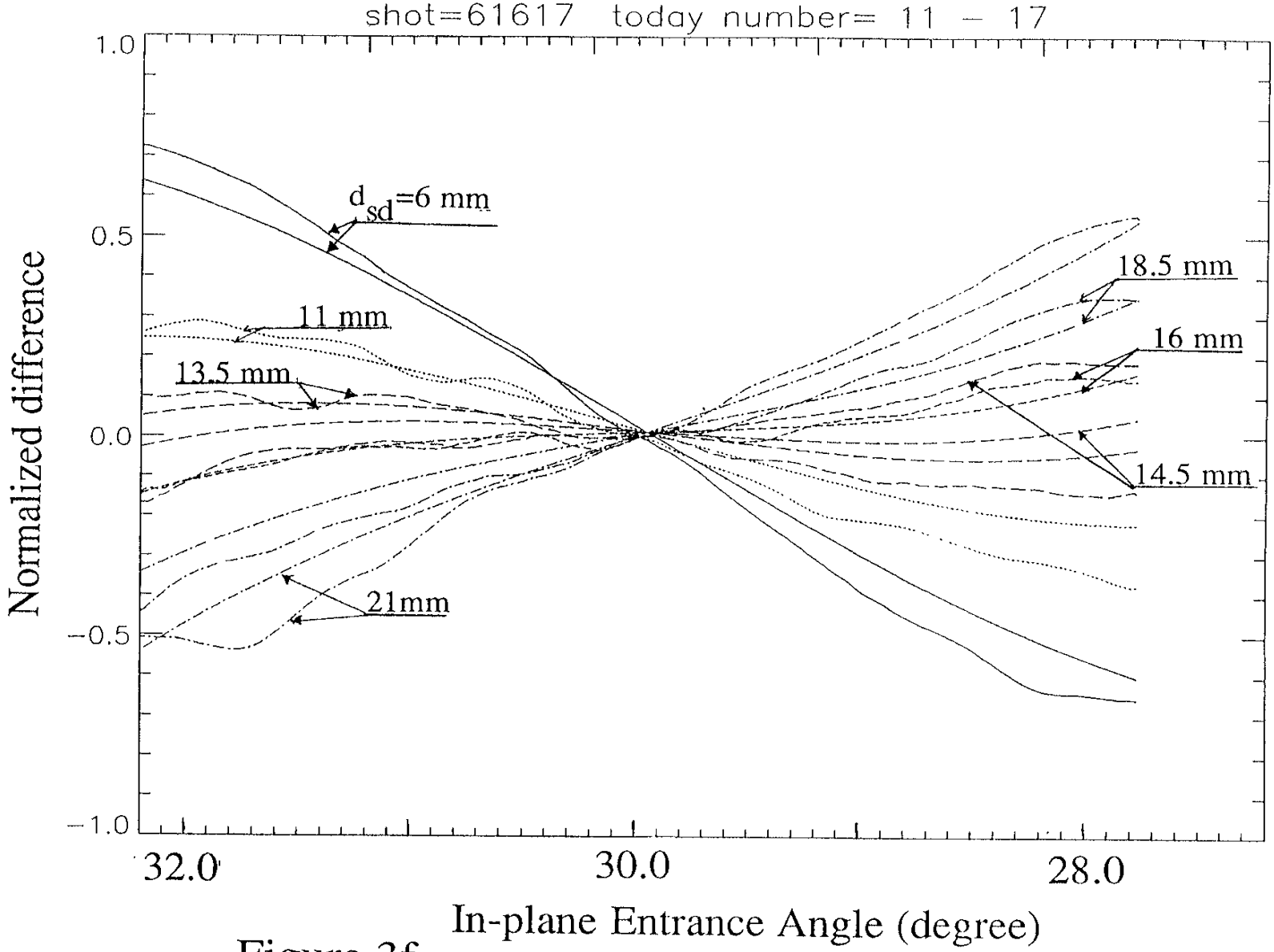
shot=61617 today number= 11 - 17
1.0
0.5
0.0
−0.5
−1.0
Normalized difference
d_{sd}=6 mm
11 mm
13.5 mm
18.5 mm
16 mm
14.5 mm
21mm
32.0
30.0
28.0
In-plane Entrance Angle (degree)

Figure 3f

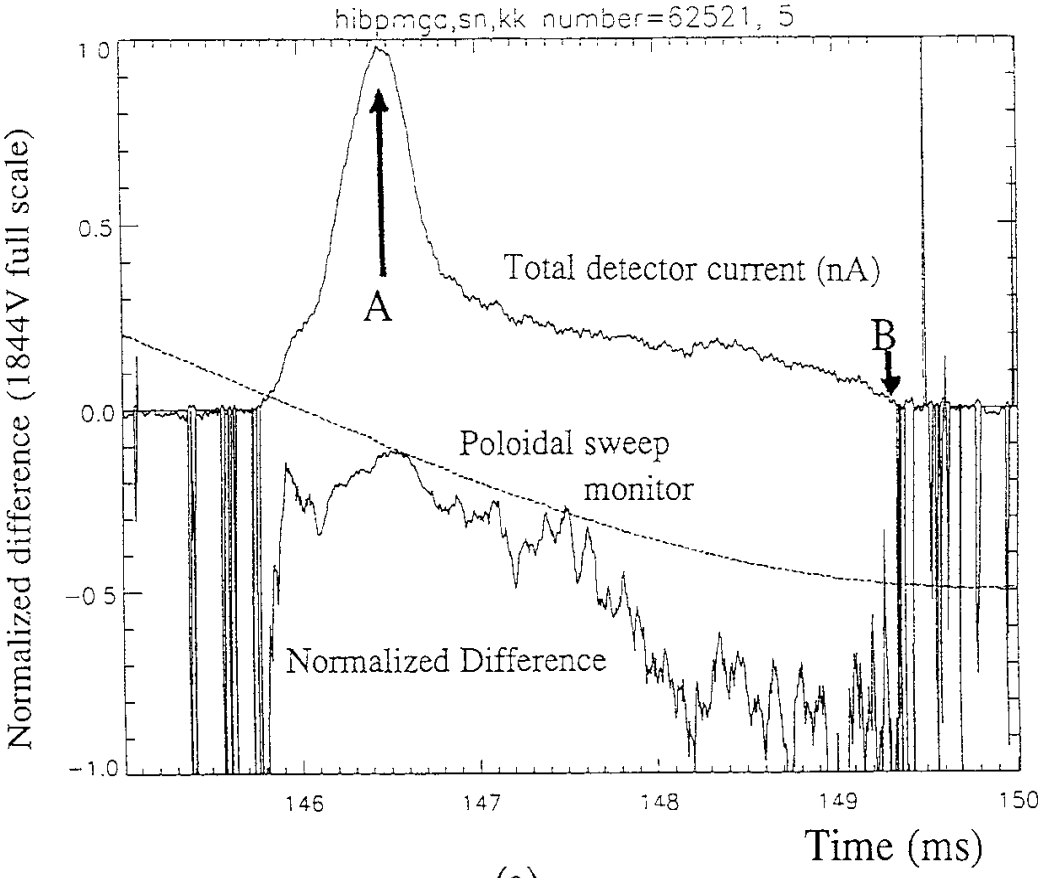
hibpmcc,sn,kk number=62521, 5
Normalized difference (1844V full scale)
1.0
0.5
0.0
-0.5
-1.0
A
B
Total detector current (nA)
Poloidal sweep monitor
Normalized Difference
146
147
148
149
150
Time (ms)

(a)

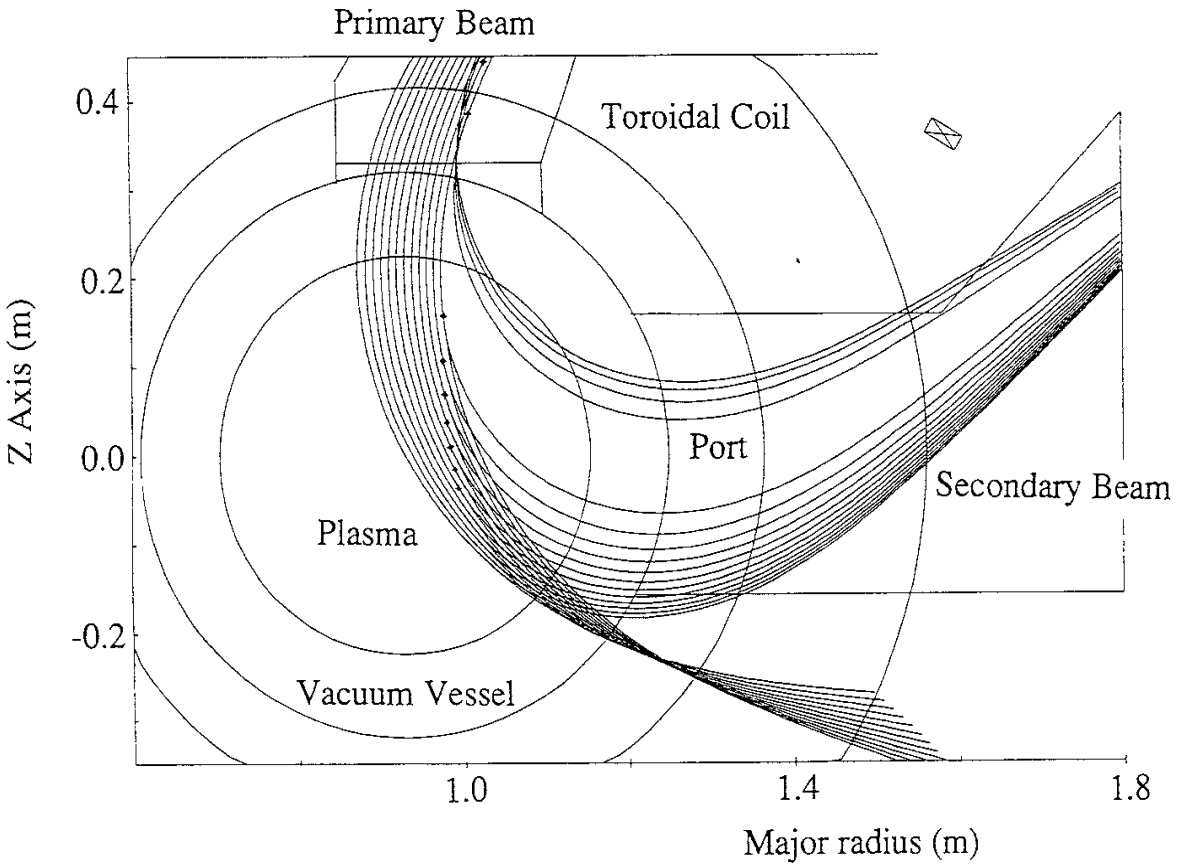
Primary Beam
Toroidal Coil
Port
Secondary Beam
Plasma
Vacuum Vessel
Z Axis (m)
0.4
0.2
0.0
-0.2
1.0
1.4
1.8
Major radius (m)

(b)

Figure 4

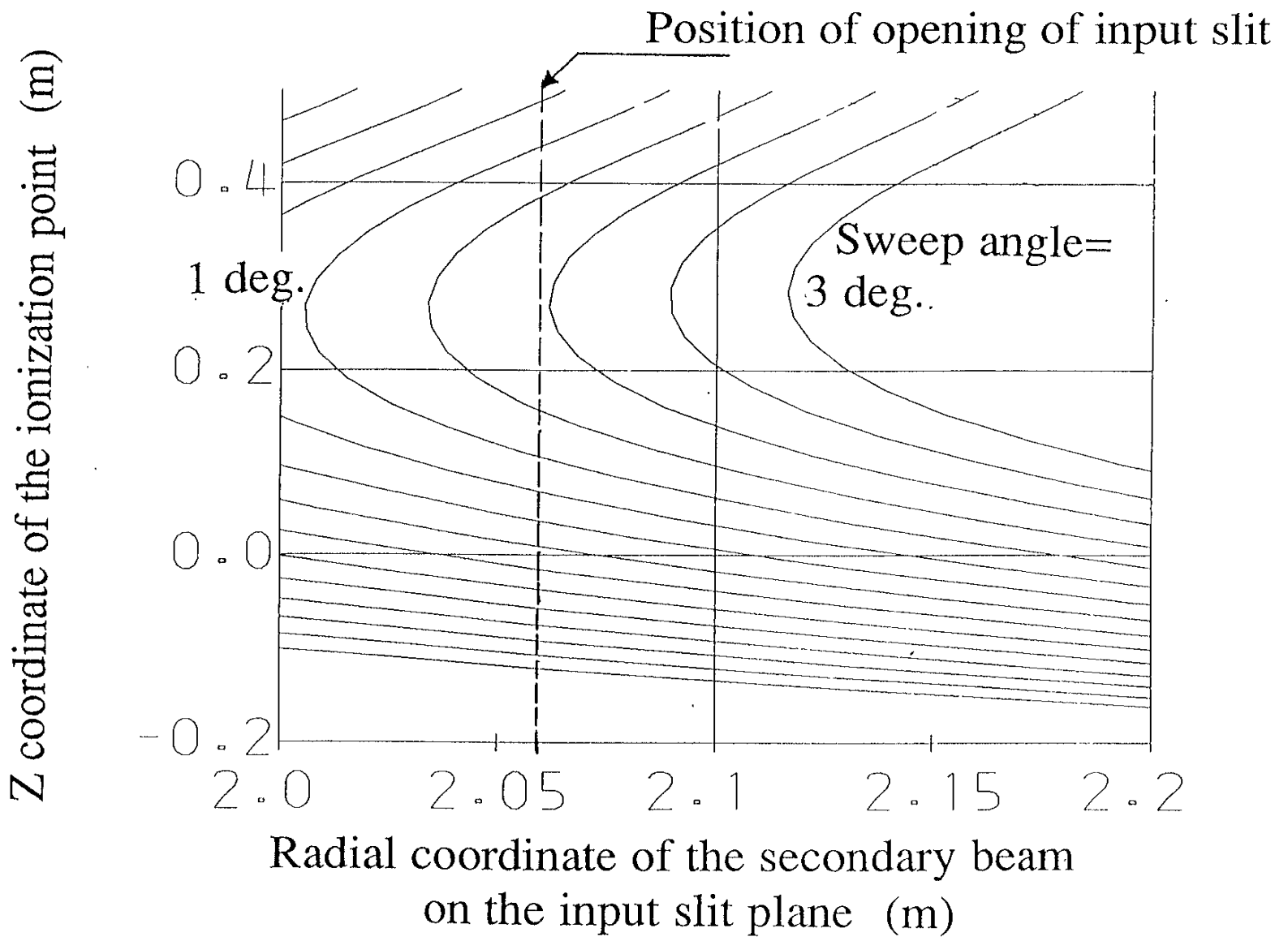
Position of opening of input slit
Z coordinate of the ionization point (m)
0.4
0.2
0.0
-0.2
1 deg.
Sweep angle=
3 deg.
2.0
2.05
2.1
2.15
2.2
Radial coordinate of the secondary beam
on the input slit plane (m)

Figure 4c

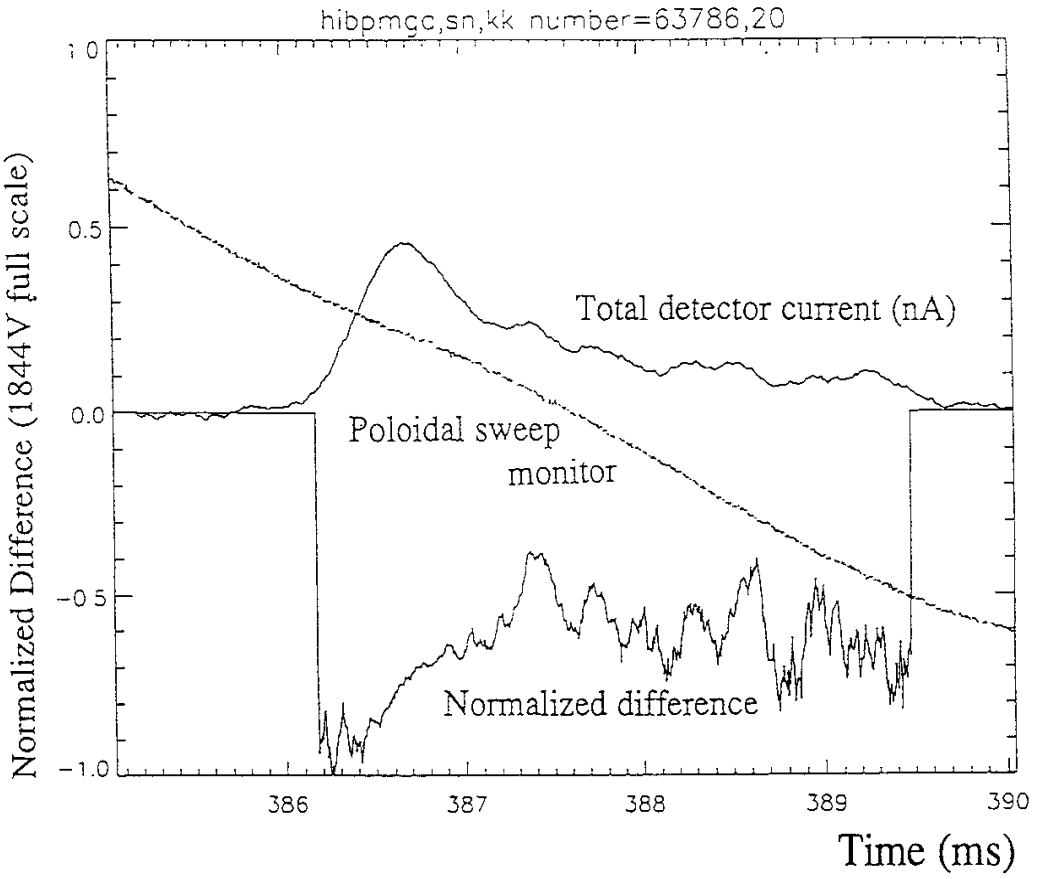

Figure 5

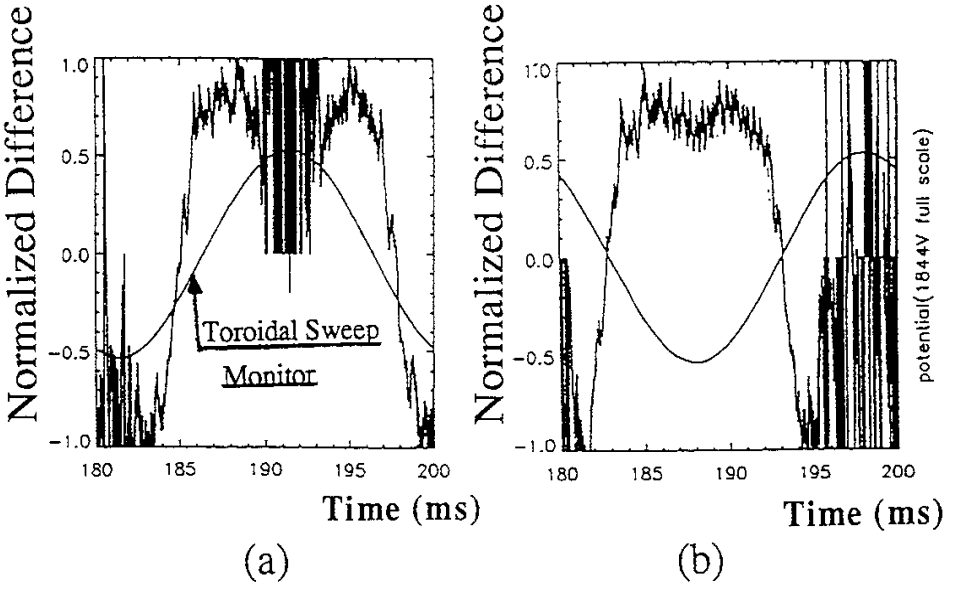

Figure 6

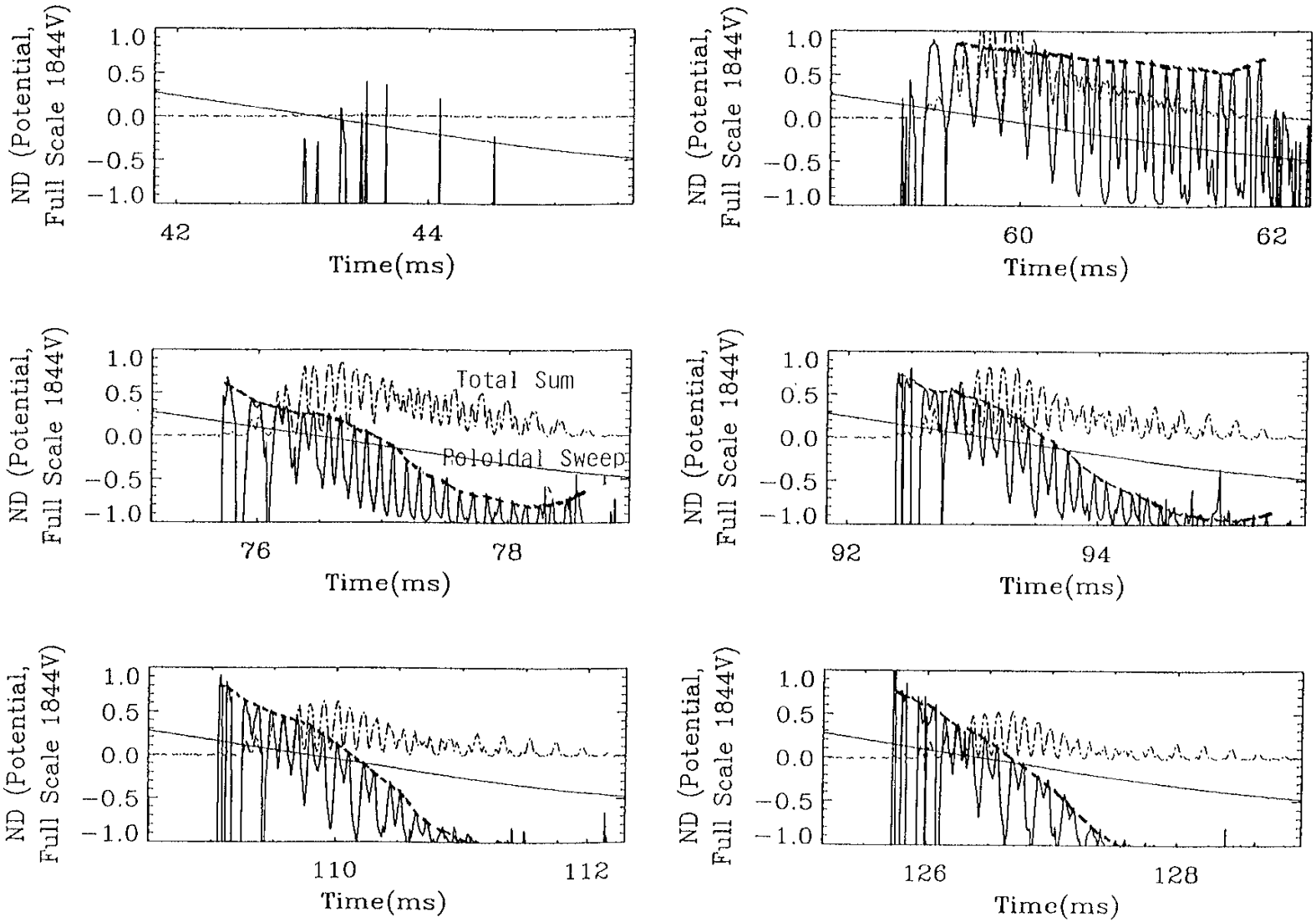
ND (Potential, Full Scale 1844V)
1.0
0.5
0.0
−0.5
−1.0
42
44
Time(ms)
60
62
Total Sum
Poloidal Sweep
76
78
92
94
110
112
126
128

Figure 7a

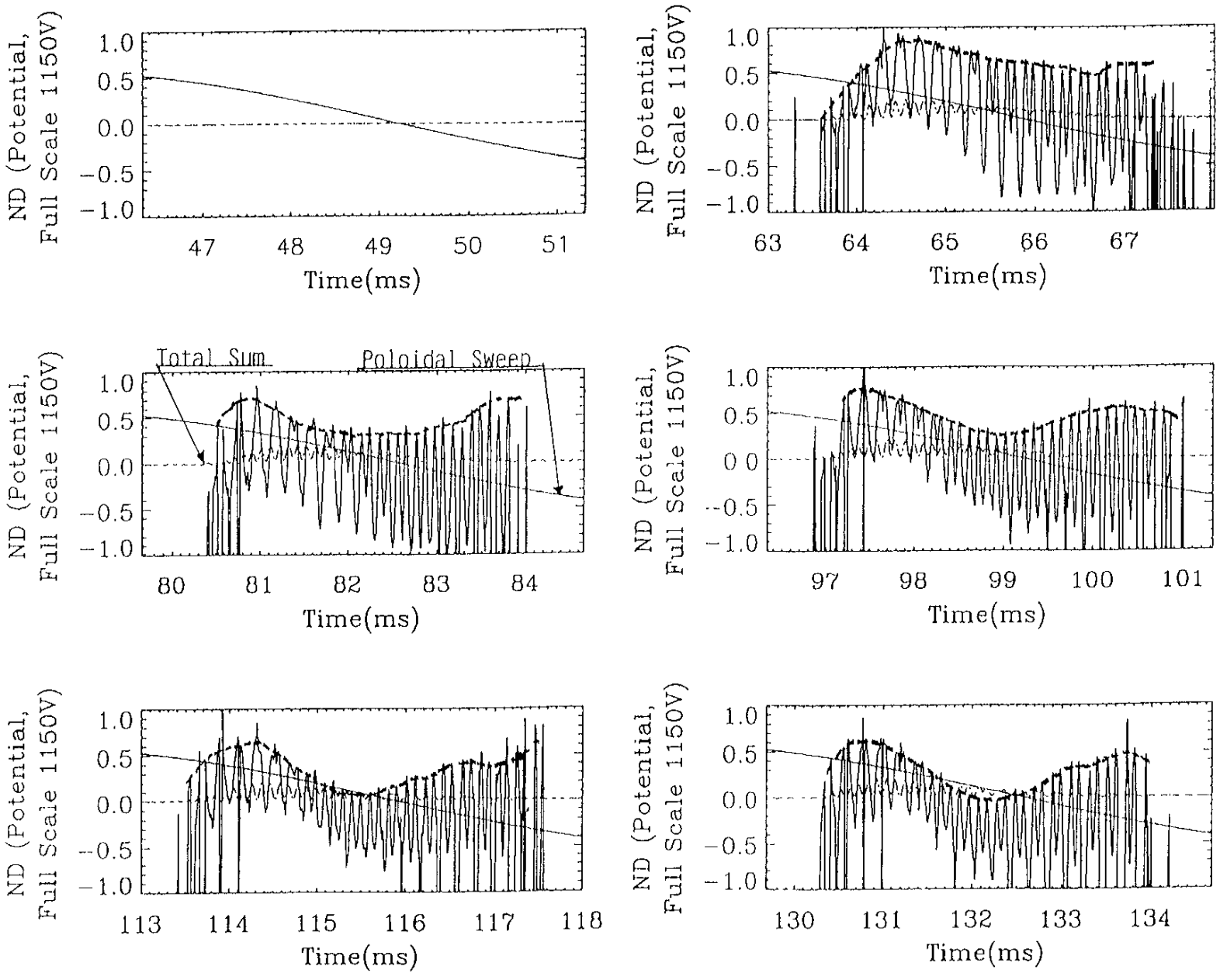
ND (Potential, Full Scale 1150V)
1.0
0.5
0.0
−0.5
−1.0
47
48
49
50
51
Time(ms)
63
64
65
66
67
Time(ms)
Total Sum
Poloidal Sweep
80
81
82
83
84
Time(ms)
97
98
99
100
101
Time(ms)
113
114
115
116
117
118
Time(ms)
130
131
132
133
134
Time(ms)

Figure 7b

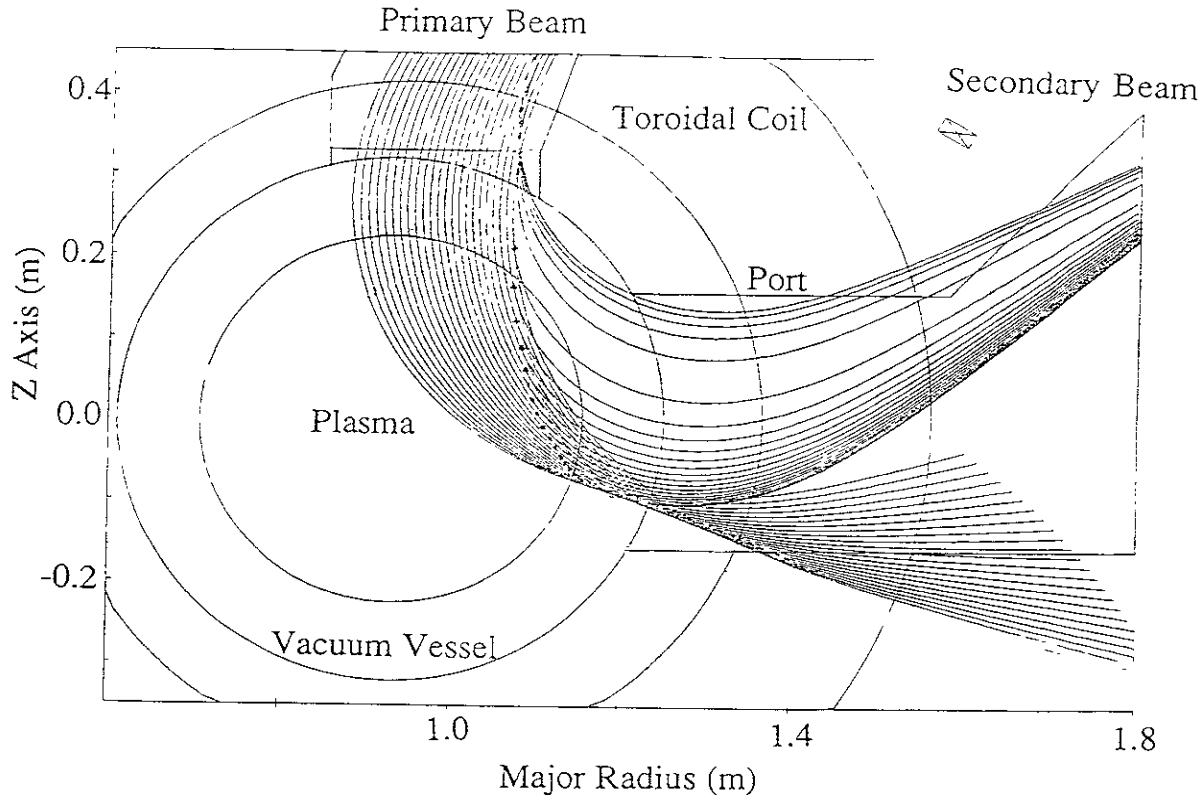
Primary Beam
Secondary Beam
Toroidal Coil
Port
Plasma
Vacuum Vessel
Z Axis (m)
0.4
0.2
0.0
-0.2
1.0
1.4
1.8
Major Radius (m)

(c)

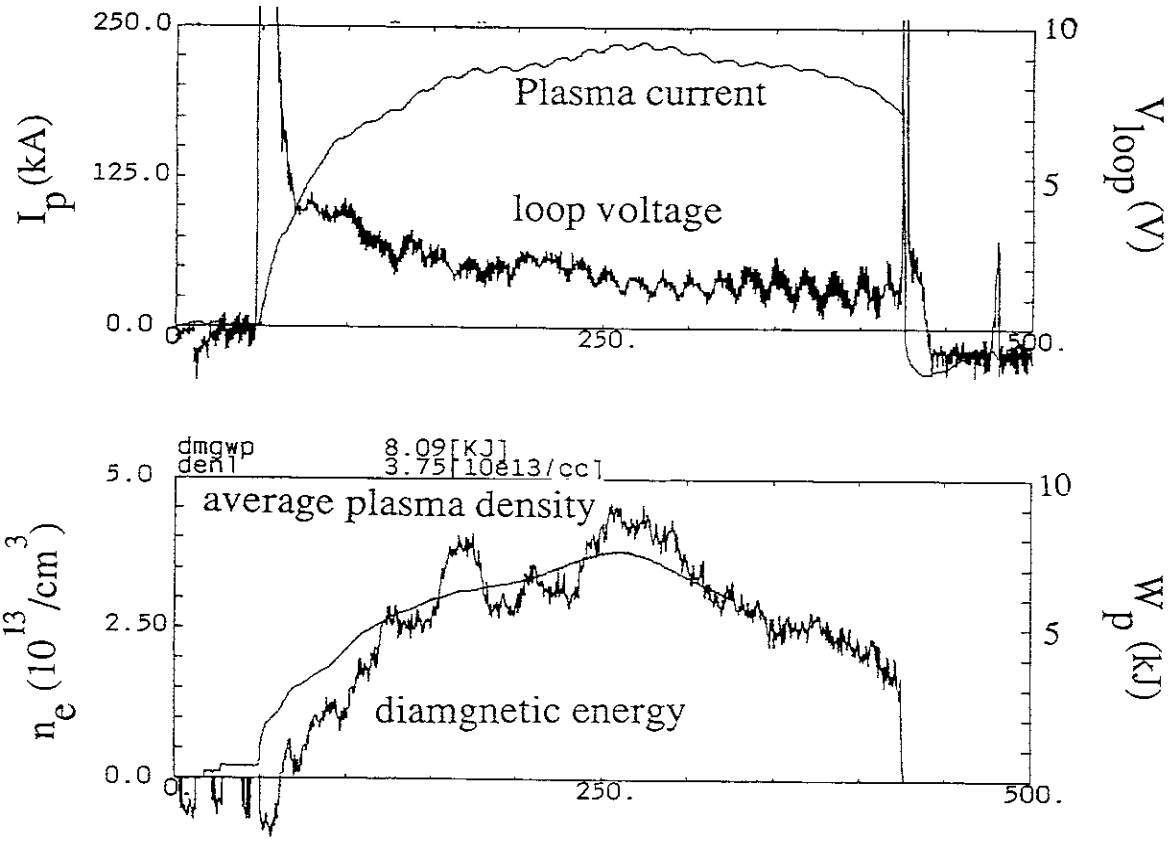
250.0
125.0
0.0
Plasma current
loop voltage
I_p (kA)
V_{loop} (V)
10
5
250.
500.
dmgwp 8.09[KJ]
den1 3.75[10e13/cc]
5.0
2.50
0.0
average plasma density
diamgnetic energy
n_e (10^{13}/cm^3)
W_p (kJ)
10
5
0.
250.
500.

(d)

Figure 7

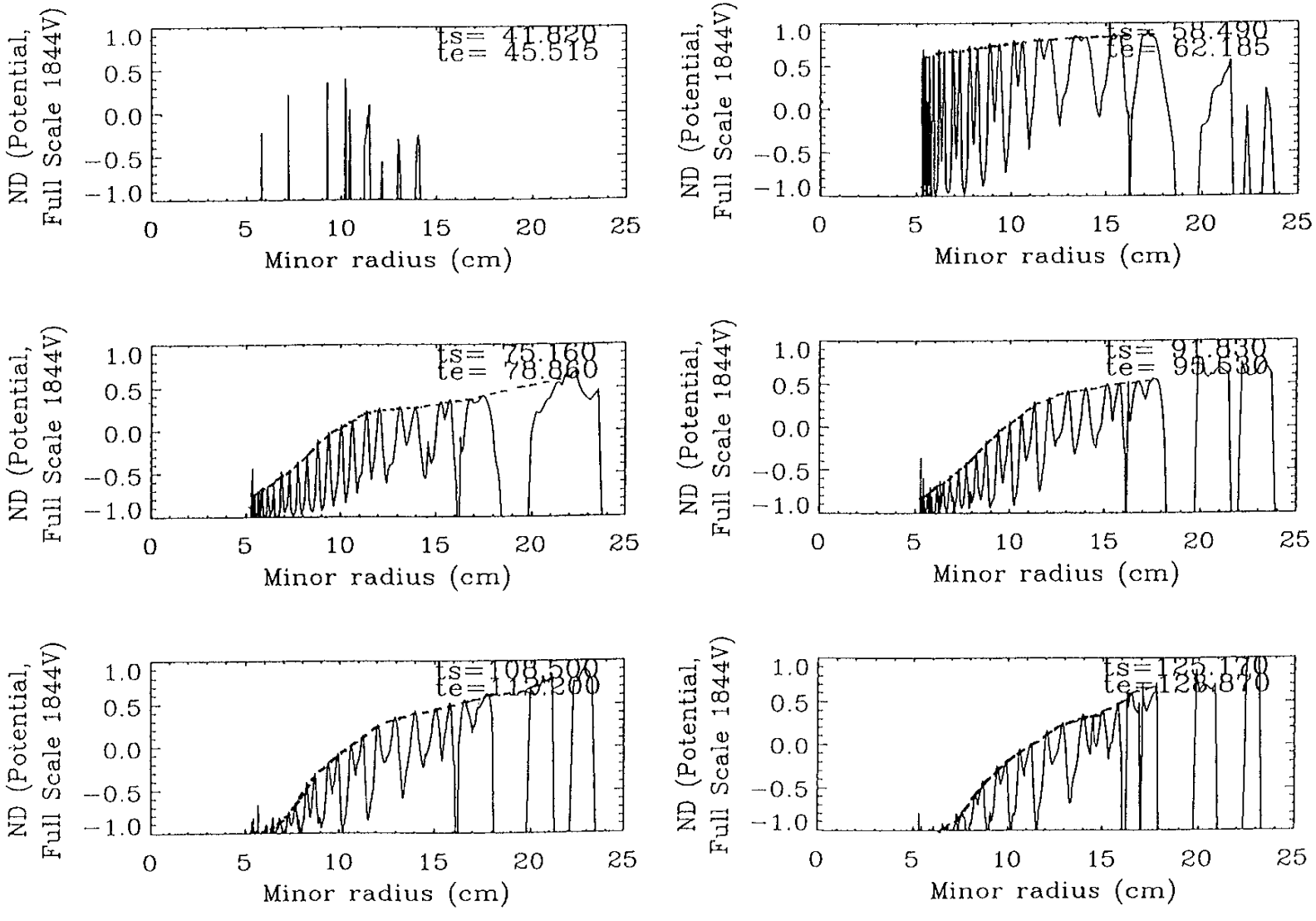
ts= 41.820
te= 45.515
ts= 58.490
te= 62.185
ts= 75.160
te= 78.860
ts= 91.830
te= 95.530
ts=108.500
te=112.200
ts=125.170
te=128.870
ND (Potential, Full Scale 1844V)
Minor radius (cm)
1.0
0.5
0.0
−0.5
−1.0
0
5
10
15
20
25

Figure 8

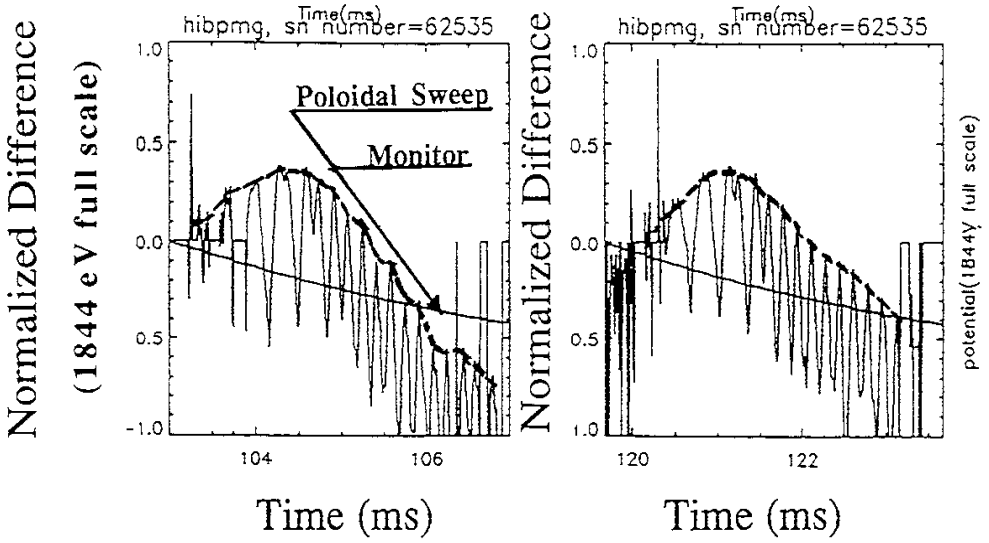
Normalized Difference
(1844 eV full scale)
hibpmg, sn number=62535
Time(ms)
Poloidal Sweep
Monitor
1.0
0.5
0.0
0.5
-1.0
104
106
Time (ms)
Normalized Difference
hibpmg, sn number=62535
Time(ms)
1.0
0.5
0.0
0.5
1.0
120
122
Time (ms)
potential(1844V full scale)

(a)

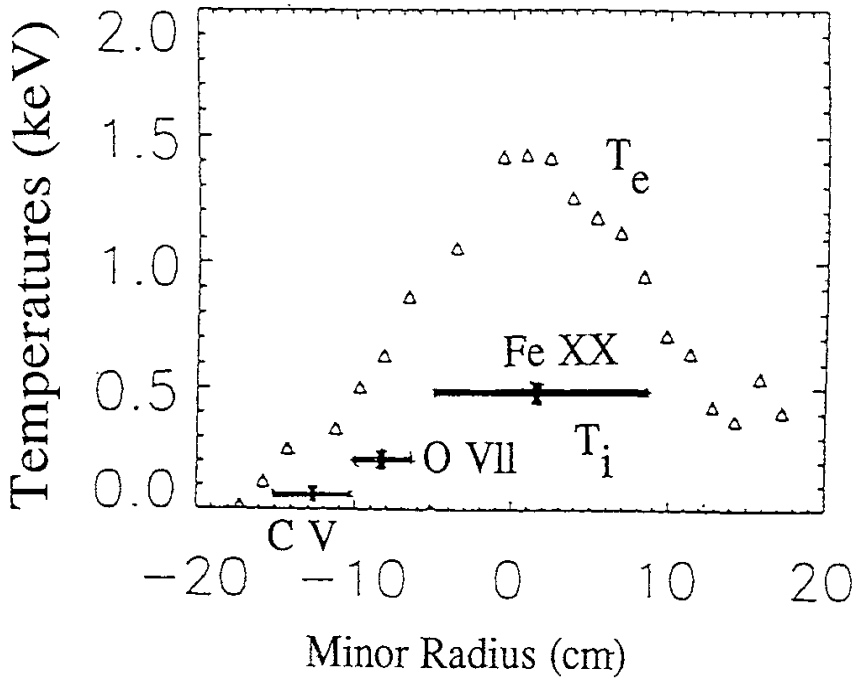
Temperatures (keV)
2.0
1.5
1.0
0.5
0.0
T_e
Fe XX
O VII
T_i
C V
−20
−10
0
10
20
Minor Radius (cm)

(b)

Figure 9

Recent Issues of NIFS Series

NIFS-225 H. Hojo and T. Hatori, *Bounce Resonance Heating and Transport in a Magnetic Mirror;* May 1993

NIFS-226 S.-I. Iton, K. Itoh, A. Fukuyama, M. Yagi, *Theory of Anomalous Transport in H-Mode Plasmas;* May 1993

NIFS-227 T. Yamagishi, *Anomalous Cross Field Flux in CHS ;* May 1993

NIFS-228 Y. Ohkouchi, S. Sasaki, S. Takamura, T. Kato, *Effective Emission and Ionization Rate Coefficients of Atomic Carbons in Plasmas;* June 1993

NIFS-229 K. Itoh, M. Yagi, A. Fukuyama, S.-I. Itoh and M. Azumi, *Comment on 'A Mean Field Ohm's Law for Collisionless Plasmas;* June 1993

NIFS-230 H. Idei, K. Ida, H. Sanuki, H. Yamada, H. Iguchi, S. Kubo, R. Akiyama, H. Arimoto, M. Fujiwara, M. Hosokawa, K. Matsuoka, S. Morita, K. Nishimura, K. Ohkubo, S. Okamura, S. Sakakibara, C. Takahashi, Y. Takita, K. Tsumori and I. Yamada, *Transition of Radial Electric Field by Electron Cyclotron Heating in Stellarator Plasmas;* June 1993

NIFS-231 H.J. Gardner and K. Ichiguchi, *Free-Boundary Equilibrium Studies for the Large Helical Device*, June 1993

NIFS-232 K. Itoh, S.-I. Itoh, A. Fukuyama, H. Sanuki and M. Yagi, *Confinement Improvement in H-Mode-Like Plasmas in Helical Systems*, June 1993

NIFS-233 R. Horiuchi and T. Sato, *Collisionless Driven Magnetic Reconnection*, June 1993

NIFS-234 K. Itoh, S.-I. Itoh, A. Fukuyama, M. Yagi and M. *Azumi, Prandtl Number of Toroidal Plasmas;* June 1993

NIFS-235 S. Kawata, S. Kato and S. Kiyokawa , *Screening Constants for Plasma;* June 1993

NIFS-236 A. Fujisawa and Y. Hamada, *Theoretical Study of Cylindrical Energy Analyzers for MeV Range Heavy Ion Beam Probes;* July 1993

NIFS-237 N. Ohyabu, A. Sagara, T. Ono, T. Kawamura and O. Motojima, *Carbon Sheet Pumping;* July 1993

NIFS-238 K. Watanabe, T. Sato and Y. Nakayama, *Q-profile Flattening due to Nonlinear Development of Resistive Kink Mode and Ensuing Fast*

Crash in Sawtooth Oscillations; July 1993

NIFS-239 N. Ohyabu, T. Watanabe, Hantao Ji, H. Akao, T. Ono, T. Kawamura, K. Yamazaki, K. Akaishi, N. Inoue, A. Komori, Y. Kubota, N. Noda, A. Sagara, H. Suzuki, O. Motojima, M. Fujiwara, A. Iiyoshi, *LHD Helical Divertor;* July 1993

NIFS-240 Y. Miura, F. Okano, N. Suzuki, M. Mori, K. Hoshino, H. Maeda, T. Takizuka, JFT-2M Group, K. Itoh and S.-I. Itoh, *Ion Heat Pulse after Sawtooth Crash in the JFT-2M Tokamak;* Aug. 1993

NIFS-241 K. Ida, Y.Miura, T. Matsuda, K. Itoh and JFT-2M Group, *Observation of non Diffusive Term of Toroidal Momentum Transport in the JFT-2M Tokamak;* Aug. 1993

NIFS-242 O.J.W.F. Kardaun, S.-I. Itoh, K. Itoh and J.W.P.F. Kardaun, *Discriminant Analysis to Predict the Occurrence of ELMS in H-Mode Discharges;* Aug. 1993

NIFS-243 K. Itoh, S.-I. Itoh, A. Fukuyama, *Modelling of Transport Phenomena;* Sep. 1993

NIFS-244 J. Todoroki, *Averaged Resistive MHD Equations;* Sep. 1993

NIFS-245 M. Tanaka, *The Origin of Collisionless Dissipation in Magnetic Reconnection;* Sep. 1993

NIFS-246 M. Yagi, K. Itoh, S.-I. Itoh, A. Fukuyama and M. Azumi, *Current Diffusive Ballooning Mode in Seecond Stability Region of Tokamaks;* Sep. 1993

NIFS-247 T. Yamagishi, *Trapped Electron Instabilities due to Electron Temperature Gradient and Anomalous Transport;* Oct. 1993

NIFS-248 Y. Kondoh, *Attractors of Dissipative Structure in Three Disspative Fluids;* Oct. 1993

NIFS-249 S. Murakami, M. Okamoto, N. Nakajima, M. Ohnishi, H. Okada, *Monte Carlo Simulation Study of the ICRF Minority Heating in the Large Helical Device;* Oct. 1993

NIFS-250 A. Iiyoshi, H. Momota, O. Motojima, M. Okamoto, S. Sudo, Y. Tomita, S. Yamaguchi, M. Ohnishi, M. Onozuka, C. Uenosono, *Innovative Energy Production in Fusion Reactors;* Oct. 1993

NIFS-251 H. Momota, O. Motojima, M. Okamoto, S. Sudo, Y. Tomita, S. Yamaguchi, A. Iiyoshi, M. Onozuka, M. Ohnishi, C. Uenosono, *Characteristics of D-^{3}He Fueled FRC Reactor: ARTEMIS-L,* Nov. 1993

NIFS-252 Y. Tomita, L.Y. Shu, H. Momota, *Direct Energy Conversion System for D-^{3}He Fusion,* Nov. 1993

NIFS-253 S. Sudo, Y. Tomita, S. Yamaguchi, A. Iiyoshi, H. Momota, O. Motojima, M. Okamoto, M. Ohnishi, M. Onozuka, C. Uenosono, *Hydrogen Production in Fusion Reactors,* Nov. 1993

NIFS-254 S. Yamaguchi, A. Iiyoshi, O. Motojima, M. Okamoto, S. Sudo, M. Ohnishi, M. Onozuka, C. Uenosono, *Direct Energy Conversion of Radiation Energy in Fusion Reactor,* Nov. 1993

NIFS-255 S. Sudo, M. Kanno, H. Kaneko, S. Saka, T. Shirai, T. Baba, *Proposed High Speed Pellet Injection System "HIPEL" for Large Helical Device* Nov. 1993

NIFS-256 S. Yamada, H. Chikaraishi, S. Tanahashi, T. Mito, K. Takahata, N. Yanagi, M. Sakamoto, A. Nishimura, O. Motojima, J. Yamamoto, Y. Yonenaga, R. Watanabe, *Improvement of a High Current DC Power Supply System for Testing the Large Scaled Superconducting Cables and Magnets*; Nov. 1993

NIFS-257 S. Sasaki, Y. Uesugi, S. Takamura, H. Sanuki, K. Kadota, *Temporal Behavior of the Electron Density Profile During Limiter Biasing in the HYBTOK-II Tokamak*; Nov. 1993

NIFS-258 K. Yamazaki, H. Kaneko, S. Yamaguchi, K.Y. Watanabe, Y.Taniguchi, O.Motojima, LHD Group, *Design of Central Control System for Large Helical Device (LHD)*; Nov. 1993

NIFS-259 K. Yamazaki, H. Kaneko, S. Yamaguchi, K.Y. Watanabe, Y.Taniguchi, O.Motojima, LHD Group, *Design of Central Control System for Large Helical Device (LHD)*; Nov. 1993

NIFS-260 B.V.Kuteev, *Pellet Ablation in Large Helical Device*; Nov. 1993

NIFS-261 K. Yamazaki, *Proposal of "MODULAR HELIOTRON': Advanced Modular Helical System Compatible with Closed Helical Divertor*; Nov. 1993

NIFS-262 V.D.Pustovitov,
Some Theoretical Problems of Magnetic Diagnostics in Tokamaks and Stellarators; Dec. 1993

NIFS-263 A. Fujisawa, H. Iguchi, Y. Hamada
A Study of Non-Ideal Focus Properties of 30° Parallel Plate Energy Analyzers; Dec. 1993

NIFS-264 K. Masai,
Nonequilibria in Thermal Emission from Supernova Remnants; Dec. 1993

NIFS-265 K. Masai, K. Nomoto,
X-Ray Enhancement of SN 1987A Due to Interaction with its Ring-like Nebula; Dec. 1993

NIFS-266 J. Uramoto
A Research of Possibility for Negative Muon Production by a Low Energy Electron Beam Accompanying Ion Beam; Dec. 1993

NIFS-267 H. Iguchi, K. Ida, H. Yamada, K. Itoh, S.-I. Itoh, K. Matsuoka, S. Okamura, H. Sanuki, I. Yamada, H. Takenaga, K. Uchino, K. Muraoka,
The Effect of Magnetic Field Configuration on Particle Pinch Velocity in Compact Helical System (CHS); Jan. 1993

NIFS-268 T. Shikama, C. Namba, M. Kosuda, Y. Maeda,
Development of High Time-Resolution Laser Flash Equipment for Thermal Diffusivity Measurements Usting Miniature-Size Specimens; Jan. 1994

NIFS-269 T. Hayashi, T. Sato, P. Merkel, J. Nührenberg, U. Schwenn,
Formation and 'Self-Healing' of Magnetic Islands in Finite-β Helias Equilibria; Jan. 1994

NIFS-270 S. Murakami, M. Okamoto, N. Nakajima, T. Mutoh,
Efficiencies of the ICRF Minority Heating in the CHS and LHD Plasmas; Jan. 1994

NIFS-271 Y. Nejoh, H. Sanuki,
Large Amplitude Langmuir and Ion-Acoustic Waves in a Relativistic Two-Fluid Plasma; Feb. 1994

NIFS-272 A. Fujisawa, H. Iguchi, A. Taniike, M. Sasao, Y. Hamada,
A 6MeV Heavy Ion Beam Probe for the Large Helical Device; Feb. 1994